UNIVERSITÀ DEGLI STUDI DI PALERMO

Dottorato di Ricerca in Scienze della Terra e del Mare

Dipartimento di Scienze della Terra e del Mare

SSD GEOS-02/C

METHOD FOR ASSESSING COASTAL VULNERABILITY TO EROSION

Ph.D STUDENT

SAMANTA BUTTO'

COORDINATOR

PROF. CHRISTIAN CONOSCENTI

TUTOR

PROF. FABRIZIO PEPE

CO-TUTOR

PROF.SSA CARLA LUCIA FARACI

CYCLE XXXVII

YEAR OF QUALIFICATION 2024

CONTENTS

Abstract

This research project provided 1) a method to evaluate the Longshore sediment transport (LST), a crucial process that shapes the coastal environments, and 2) an index designed to assess the vulnerability of coastal areas to erosion at the beach scale.

In the first study, I evaluated the predictive capacity of three widely used empirical formulas (CERC, 1984; Kamphuis, 1991; Van Rijn, 2014) and the XBeach 2DH numerical model for estimating the LST rate by comparing the results obtained from both methods with field LST data. I have chosen three coastal areas in Malta Island (Għadira Bay) and northern Sicily (Cefalù and Campofelice di Roccella sites) based on different characteristics in terms of sediments, coastal type (open or embayed) and morpho-bathymetry. For each site, I analysed wave parameters, grain size of the beach and seabed sediments, coastal morphology, and marine vegetation distribution. Furthermore, I used field measurements to calibrate the numerical model's sediment transport and morphological parameters. The research findings showed that the calibrated numerical model provides greater accuracy in LST rate estimation than the empirical formulas. The latter overestimated the LST rates by factors ranging from 435 to 7885. In contrast, the numerical model overestimated the LST rate by factors of 1.8 and 1.9 at the Cefalù site and Għadira Bay, respectively, and underestimated by a factor of 0.5 at the Campofelice di Roccella site. The good performance of the numerical model is due to its consideration of site-specific factors that influence the LST rate. The parameter values for the model calibration can be used successfully in embayed systems characterized by fine/coarse sandy beaches. Moreover, the numerical model, tested so far only for sandy beaches, also works well on gravelly beaches.

In the second study, I focused on developing a Coastal Vulnerability Index (CVI) to erosion at the beach scale. The proposed CVI integrates natural and physical factors represented as four sub-indexes (Morphological Characteristics, Shoreline Displacement, Longshore Sediment Transport and Wave Height) that control coastal erosion. I analysed the sub-indexes through a comprehensive dataset, including aerial surveys, digital elevation models, and wave climate data, supported by numerical modelling through the XBeach 2DH model. I tested the method at the Għadira Bay, a pocket beach located in northeastern Malta. Results revealed that the coastline is affected by low vulnerability to erosion in the north and central sectors and moderate in the southern. The CVI developed in this study significantly improves previous methodologies by offering a more precise representation of beach

vulnerability to erosion through 1) the consideration of the headland's length and the marine vegetation as parameters affecting the balance between sediment loss and input; 2) a quantitative evaluation of the LST sub-index. The proposed CVI offers a comprehensive and reliable approach to quantify coastal erosion risk, providing an essential tool for local governments to improve coastal management strategies and mitigate risks associated with coastal erosion.

Introduction

The coastal environment experiences rapid changes in its physical and geomorphological features, driven by a dynamic interplay of both natural and anthropic factors. Increased populations, economic activities along coastlines, and rising sea levels during the 21st century, as projected by the Intergovernmental Panel on Climate Change, have heightened the focus on coastal evolutionary processes and coastal vulnerability (CV). This dynamic emphasises the need for dedicated assessment tools for CV.

A literature review indicates that several methods have been proposed for the CV assessment. Some approaches focus on analysing vulnerability components (e.g., geological, physical, and socio-economic) to provide a CV index (CVI) at various time and spatial scales. Other methods use numerical models to investigate the hydrodynamic and morphodynamic impacts of storm events at the scale of a single beach. However, these methods often do not incorporate the analysis of sedimentary dynamics in the submerged marine sector, which is influenced by biotic and abiotic factors (e.g. waves, currents and marine vegetation). Integrating data from studies on the processes influencing CV in coastal and marine environments is essential for comprehending the evolution of coastal areas over time and obtaining comprehensive results.

This research project is divided into two studies that provide 1) a method to evaluate the Longshore sediment transport (LST), a crucial process that shapes the coastal environments, and 2) an index designed to assess the vulnerability of coastal areas to erosion at the beach scale. The results of these studies are summarized in two scientific papers jointly authored by several contributors.

The first study deals with the predictive capacity of three widely used empirical formulas (CERC, 1984; Kamphuis, 1991; Van Rijn, 2014) and the XBeach 2DH numerical model for estimating the LST rate by comparing the results obtained from both methods with field LST data. The investigated coastal areas are located on Malta Island (Għadira Bay) and northern Sicily (Cefalù and Campofelice di Roccella sites). These sites were selected based on their varied characteristics, which include sediment grain size, coastal morphology and marine vegetation cover.

The second study focuses on developing a Coastal Vulnerability Index (CVI) to erosion at the beach scale. The proposed approach relies on numerical approximations and quantitative/qualitative assessment of physical and geological indexes that govern beach evolution. Sub-indexes include Morphological Characteristics (MC), Shoreline displacement (SD), Longshore Sediment Transport (LST) and Wave Height (WH). The proposed methodology involves four steps. The first step regards the collection of an extensive dataset (aerial photographs, digital elevation models, GPS data, wave data, longshore sediment transport data and grain-size data) to characterize the beach and split it into sections during the second step. The third step consists of the calculation of the proposed sub-indexes. This research approach is tested on Għadira Bay (GB) in Malta.

This research highlights the importance of selecting a LST estimation method based on site-specific characteristics and provides insight into sedimentary input/output processes, contributing to a broader understanding of CV by examining different beaches. This approach ensures the adaptability and effectiveness of the proposed methodologies across different coastal settings. Furthermore, CV maps facilitate informed decision-making for planning strategies related to population protection, infrastructure preservation, cultural heritage conservation, and maintaining natural habitats in coastal areas.

Specific contributions of the candidate to the research

My contribution to the two scientific papers was pivotal in the conceptualization, data curation, formal analysis, and manuscript preparation. Specifically, I led the conceptualization of the research, collected and processed the data, performed detailed analyses, and drafted the original versions of both papers. These activities allowed me to develop skills in (1) the development, calibration, and application of numerical models for estimating coastal sediment transport and analyzing coastal morphodynamics and hydrodynamics; (2) processing digital elevation models (DEMs) and orthophotos using GIS software; (3) collecting coastal sediment transport data (using streamer trap), bathymetric data (using single-beam system), and photogrammetric and topographic data (via autonomous vehicles and GNSS receivers); (4) conducting granulometric analyses of sandy and gravelly sediment samples; (5) performing statistical analyses of data series, such as wave data; and (6) designing and applying coastal erosion vulnerability indices.

I carried out some of these activities independently (e.g., granulometric and statistical analysis of wave data, development of vulnerability indices, and processing of bathymetric maps). My co-authors supported me in acquiring sediment data using the streamer trap, bathymetric data with the single beam system, and photogrammetric data through the autonomous receiver. They also assisted in the processing phase of the photogrammetric data, the calibration of numerical models, and the review and editing of the papers.

CHAPTER 1

Evaluating Longshore Sediment Transport: a comparison between empirical formulas and XBeach 2DH numerical model

NOTE: This chapter is a scientific paper submitted to “Marine Geology”. The authors are the followings: Buttò S., Faraci C., Corradino M., Iuppa C., Colica E and Pepe F.

Abstract

Longshore sediment transport (LST) is a crucial process shaping coastal environments. In this research, we evaluate the predictive capacity of three widely used empirical formulas (CERC, 1984; Kamphuis, 1991; Van Rijn, 2014) and the XBeach 2DH numerical model for estimating the LST rate by comparing the results obtained from both methods with field LST data.

We chose three coastal areas in Malta Island (Għadira Bay) and northern Sicily (Cefalù and Campofelice di Roccella sites) based on different characteristics in terms of sediments, coastal type (open or embayed) and morpho-bathymetry.

For each site, we analysed wave parameters, grain size of the beach and seabed sediments, coastal morphology, and marine vegetation distribution. Furthermore, we used field measurements to calibrate the numerical model's sediment transport and morphological parameters.

Our findings show that the calibrated numerical model provides greater accuracy in LST rate estimation than the empirical formulas. The latter overestimates the LST rates by factors ranging from 435 to 7885, whereas the numerical model overestimates the LST rate by factors of 1.8 and 1.9 at the Cefalù site and Għadira Bay, respectively, and underestimates by a factor of 0.5 at the Campofelice di Roccella site.

The good performance of the numerical model is due to its consideration of site-specific factors that influence the LST rate. The parameter values for the model calibration can be used successfully in embayed systems characterized by fine/coarse sandy beaches. Moreover, the numerical model, tested so far only for sandy beaches, also works well on gravelly beaches.

Keywords: Longshore sediment transport, Coastal erosion, Empirical formulas, XBeach 2DH numerical model

1. Introduction

Longshore sediment transport (LST) is a natural process that influences the dynamics and evolution of coastal environments. Various factors, including the site's sedimentological, morphological, and biotic components, significantly determine the LST rate (Pereira Quadrado & Goulart, 2020; Salem Cherif et al., 2019; Widdows & Brinsley, 2002). In embayed systems, the bathymetry of the inner shelf (Dolique & Anthony, 2005) and the dimensions of the headlands (King et al., 2021) influence sediment retention even under conditions of strong currents and waves (Dehouck et al., 2009). Whereas vegetation on the seabed reduces the shear stress at the sediment-water interface and thus the sediment erosion (Le Hir et al., 2007; Widdows & Brinsley, 2002).

The main approaches for estimating the LST rate are typically empirical formulas and numerical models. Empirical formulas, such as bulk transport formulas, represent physical processes through explicit equations based on easily available input parameters (e.g., wave height and water depth at the breaking point, wave period, breaking wave angle, median sediment grain size, seabed slope, water, and sediment density) and empirical coefficients (Bailard, 1981; Bayram et al., 2007; Walton et al., 1989). However, most formulas were not fully successful because they include weakly defined parameters (e.g., beach slope) or are based on a limited data set (e.g., range of grain size or wave heights). Moreover, bulk formulas are calibrated with empirical coefficients that depend on field data, so their accuracy is linked to the quality of field measurements or the specificity of the survey site.

Various formulas exist for calculating LST, differentiated by the variables they depend on, such as sediment grain size, seabed slope, wave period or water depth at breaking point. Among these, the Coastal Engineering Research Center (CERC) formula (1984) and Kamphuis's (1991) formula are widely used in both practice and fundamental research. Many researchers focused on calibration of the parameters that influence the LST rate value to improve the formulas' accuracy (Bodge & Kraus, 1991; Eversole & Fletcher, 2003; Mil-Homens et al., 2013; Pereira Quadrado & Goulart, 2020; Salem Cherif et al., 2019; Sanil Kumar et al., 2003; Shanas & Sanil Kumar, 2014; Wang et al., 1998, 2002; Williams et al., 2008). For instance, Mil-Homens et al. (2013) used the least-squares optimization algorithm to calculate a coefficient relating sand transport to longshore energy flux in the CERC (1984) formula and a series of parameters of the Kamphuis (1991) formula. Other authors also tried to improve the CERC (1984) formula by calibrating the k parameter (Bodge & Kraus, 1991; del Valle et al., 1993; Eversole & Fletcher, 2003; Schoonees & Theron, 1993; Van Wellen et al., 2000), and the Kamphuis (1991) formula by calibrating the weight of the grain size by modifying the D50 exponent (Mil-Homens et al., 2013; Tomasicchio et al., 2013; Van Rijn, 2014). Also, Van Rijn (2014) analysed the research of CERC (1984), Kamphuis (1991), and

Mil-Homens et al. (2013) and proposed a general and dimensionally correct predictive formula.

Numerical models simulate the hydrodynamic processes of short-wave transformation (refraction, shoaling, and breaking) and long-wave transformation (generation, propagation, and dissipation), compute sediment transport (both suspended and bed total load) and morphological changes (Delft3D of Lesser et al., 2004, MIKE21 of DHI, 2005 and UNIBEST of WL|Delft Hydraulics, 1994; Lesser et al., 2004). These models estimate LST by solving the fundamental equations governing fluid motion, such as the Navier-Stokes equations for incompressible flow, the shallow water equations for wave propagation, and the advection-diffusion equation for sediment transport. The models use numerical methods like finite difference or finite element techniques to solve these equations, allowing them to calculate key parameters influencing sediment transport, such as wave breaking, radiation stresses, turbulence, bed shear stress, equilibrium sediment concentration, and flow velocity.

Models differ for the spatial dimensions in which the phenomenon is described (Samaras & Koutitas, 2014). One-dimensional (1D) models (e.g. GENESIS of Hanson (1989), ONELINE of Dabees and Kamphuis (1998) and SMC of González et al. (2007)) study sediment transport along a single cross-shore transect. Two-dimensional (2D) models (e.g. Dally–Dean model of Dally and Dean (1984), UNIBEST of Roelvink and Stive (1989), LITCROSS of Hedegaard et al. (1991) and XBeach of Roelvink et al. (2009)) analysed the transport process in plane by using horizontal (2DH) or vertical (2DV) computational grids. Three-dimensional (3D) models (e.g. CH3D-SED of Gessler et al. (1999), Delft3D of Lesser et al. (2004) and GAIA-TELEMAC of Tassi et al. (2023)) integrate a sediment transport model with a hydrodynamics model to solve equations of continuity and motion over a 3D grid.

The modelling approach is more labour-intensive than the application of formulas due to its reliance on relatively detailed and numerous input data. Moreover, the model complexity frequently requires a site-specific calibration based on field data to improve the result accuracy (Bergillos et al., 2017; Elsayed & Oumeraci, 2017; Garzon et al., 2022; Hwang et al., 2024; Jin et al., 2021; McCall et al., 2010; Satheeshkumar & Balaji, 2021; Simmons et al., 2019; Simmons & Splinter, 2022). Following several studies, the calibration process should consider sediment transport parameters and morphology parameters because they are the most influent on the LST rate (Bugajny et al., 2013; Elsayed & Oumeraci, 2017; Hwang et al., 2024; Satheeshkumar & Balaji, 2021).

2D models balance result accuracy and computational time satisfactorily compared with 1D and 3D models. In particular, the 2DH numerical models are the most suitable for predicting LST rate because they consider 1) the areal morphological and hydrodynamics variability of the site compared to 1D models and 2) alongshore variations of water levels, fluid velocities and their derivatives compared to 2DV models.

Despite continuous efforts to refine the LST estimation methods, an open problem regards the accuracy of the methods used in different coastal environments. This study aims to evaluate the predictive capacity of three of the most commonly used bulk formulas: the CERC formula (1984), the Kamphuis formula (1991) and the Van Rijn formula (2014). These formulas are compared to the XBeach 2DH numerical model (D. Roelvink et al., 2009) for estimating the LST rate under non-extreme conditions. The research defines which approach provides the most accurate LST value for different coastal settings by comparing the results of the empirical formulas and the numerical model with field-acquired LST data. Furthermore, the influence of seabed vegetation on the LST rate is investigated.

The coastal areas of Għadira Bay (GB, Malta Island), Cefalù (CF, northern Sicily), and Campofelice di Roccella (CR, northern Sicily) were chosen for this study based on their different characteristics in terms of beach sediment grain size, coastal type (open or embayed system), seabed morphology, and presence of vegetation.

This research highlights the importance of selecting a LST estimation method based on site-specific characteristics. An accurate estimate of the LST value is essential for effective coastal management, erosion mitigation, and the preservation of coastal ecosystems.

The paper is organized as follows: section 2 presents the study areas; section 3 describes the materials and methods used to collect and analyse data (field measurements and wave parameters) and to calculate the LST rate (bulk formulas and XBeach 2DH model); section 4 outlines the results of the morphologic and granulometric analysis of the sites, wave conditions, marine vegetation, LST rate value for each site; section 5 discusses the bulk formulas and XBeach 2DH model's results and compares them with field observations; section 6 highlights the conclusion of this research.

2. Oceanographic and climatic conditions of the study areas

2.1 Malta Island

Malta Island is located in the central Mediterranean Sea, approximately 100 km south of Sicily (fig. 1 a). Its coastal climate is subjected to the dynamics of air pressure systems originating from the Atlantic and nearby landmasses. The storms affect the island principally during autumn and winter, driven by the convergence of low-pressure systems with warm, moist air over the Mediterranean (Galdies, 2011). A twenty-nine-year observation period reveals a mean annual surface wind speed of 16.3 km/h, with prevailing north-westerly winds dominating 20.7% of days annually (Galdies, 2011). The winds significantly shape wave patterns around the islands. The analysis of a fourteen-year dataset by the Malta Maritime Authority (Scott Wilson Kirkpatrick and Co. Ltd, 2003) indicates similar directions of offshore waves and winds, suggesting that local wind-generated waves play a more significant role than swell waves.

The wave climate has a strong seasonal energy pattern, with peak energy concentrated during the winter months from November to April (Drago et al., 2013). The annual mean significant wave height ($H_{s,m}$) is 1.22 m, increasing to 1.92 m during winter (Drago et al., 2013).

We selected the beach of GB as a study area for this research. The GB site is an embayed system located in the northeast sector of the island (fig. 1 a and e) and bounded by headlands on both sides. The beach has about 5 m thick sandy barrier bordering salt marshes and pools (Gatt, 2021). An observation period between 12 a.m. on 1 January 1993 and 11 p.m. on 31 December 2023 revealed that north-westerly waves are predominant at the GB site, with significant wave height (H_s) typically between 0.5 and 1 m, and frequencies of about 15% (fig. 2c).

2.2 Northern Sicily

The northern coast of Sicily is located in the southern Tyrrhenian Sea (fig. 1 a and b). The wind climate of this area is characterised by winds with seasonal variability, including the southwest Libeccio wind during winter, the southeast Sirocco wind during autumn and spring and the north-northwest Mistral wind typically during winter (Barbariol et al., 2021). Also, this area is characterized by winds with the highest speed variability of the Mediterranean basin during the year (Soukissian et al., 2018). In the observation period between 2015 and 2019, the maximum value of mean annual surface wind speed was about 15 m/s, with a north-northwestern direction and occurrence frequency greater than 14% (Sperati et al., 2024; https://atlanteeolico.rse-web.it/).

The wave climate is mainly controlled by regional winds and the morphological complexity of the offshore areas, resulting in limited fetches in coastal shallow regions relatively proximal to the generation areas (Barbariol et al., 2021). The trend analysis of the wave time series over 40 years shows that the highest wave power values occur during winter, in agreement with the increase of H_s in the same period (Caloiero et al., 2022).

Along the northern coast of Sicily (fig. 1 b), we selected two study areas, the CR (fig. 1c) and CF sites (fig. 1d). The CR site is an open system characterized by a 1.5 km long and 40 m wide gravel beach. Meanwhile, the CF site is an embayed system bounded by headlands on both sides. This site consists of a sandy beach, approximately 1.7 km long, limited landward by anthropic structures. An observation period between 12 a.m. on 1 January 1993 and 11 p.m. on 31 December 2023 revealed that sites CR and CF are characterized by predominance of waves from the northwest and H_s between 0.5 and 1 m that occasionally exceed 2 m (fig. 2a-b).

3. Materials and Methods

3.1. Data Collection

3.1.1 Digital Elevation Models and seafloor mapping

Digital Elevation Models (DEMs) of the emerged coastal areas of CR and CF sites were derived from LIDAR data with a resolution of 2 m, acquired during ATA flights in 2012/2013, available in the SITR portal of the Sicily Region (https://map.sitr.regione.sicilia.it/gis/services/modelli_digitali/mdt_2013/ImageServer/WCSServer). DEM of the emerged coastal area of the GB site was obtained by aerial photogrammetric data acquired by an unmanned aerial vehicle (UAV) Mavic 3 Enterprise and processed using Agisoft Metashape v. 2.0.0. The photogrammetric data were also used for the mapping of *Posidonia oceanica* in the area extending from the coastline to 10 m of depth. The map of *P. oceanica* distribution was created by using QGIS software.

Bathymetric data from zero to approximately 20 m of depth were obtained at all three sites (CR, CF, and GB) using a 235 kHz Ohmex SonarMite V5 single beam echo-sounder mounted on a small inflatable boat. These data were integrated with Topcon Hyper HR GNSS data collected in the surf zone (depth range 0 – 1.5 m). The bathymetric maps were generated by processing the single beam and GNSS data using SAGA GIS software and applying the linear ordinary Kriging interpolation method.

3.1.2 LST Rate measurement

A "streamer trap" was built based on the model proposed by Kraus (Kraus, 1987) to collect data on LST rates in the surf zone. The instrument consists of four rectangular collection bags, called streamers, that allow the capturing of sediment moving both at the seabed and in suspension (fig. 3a). The streamer's mouth is 20 cm wide and 16 cm high. The bags are made of polyester-sieve cloth with a 60 µm mesh size to trap sand to gravel size sediment. The streamers were vertically mounted on a metal frame: the lowest streamer and the uppermost one were positioned 2 cm and 75 cm from the seabed, respectively. Streamer traps have several limitations that can cause errors in the measurements. One of the major limitations is the need for continuous controls of bags that tend to wrap around the legs of the rack if the current is weak or intermittent due to oscillatory water motion caused by the passage of waves (Kraus, 1987). Another difficulty is using the streamer traps for wave-breaking heights of more than 1m due to their manual deployment and the possibility that the trap tips in the direction of forward wave motion (Kraus, 1987). Moreover, streamer traps are susceptible to both oversampling and undersampling issues. Oversampling can occur due to initial stirring, while undersampling may result from gaps between the bed and the first bag and obstruction of the bed load transport by the trap (Masselink et al., 2009).

Acquisition surveys were carried out in the study areas on 27th July 2023 (CR site), 24th January 2024 (GB site), and 2nd April 2024 (CF site, fig. 3b). The streamer trap was deployed for 10 minutes, following the procedure proposed by Kraus (1987) and adopted in subsequent studies (Cartier & Héquette, 2015; Williams et al., 2008). This duration minimizes disturbances to the bottom flow caused by the trap's presence, allowing to obtain a representative sediment sample (Pereira Quadrado & Goulart, 2020). The measurement procedure was repeated twice at each site to improve data robustness. The LST rate (Q_t) was determined by the approach proposed by Kraus (Kraus, 1987) and modified by Wang and al. (1998):

$$F_k = \frac{m_s}{t}$$

$$\Delta F_k = \left(\frac{\frac{F_{k+1}}{h_{k+1}} + \frac{F_{k-1}}{h_{k-1}}}{2} \right) * \Delta z_k$$

$$Q_t = \sum_{k=1}^{n} F_k + \sum_{k=1}^{n-1} \Delta F_k$$

where F_k is the sediment flux at streamer k (kg/s), m_s is the mass of sand at streamer k (kg), t is the sample time (s), ΔF_k is the sediment flux between two adjacent streamers (kg/s), F_{k+1} and F_{k-1} are the fluxes through the upper and lower streamers (kg/s), h_{k+1} and h_{k-1} are the vertical widths of the opening of the upper and lower streamers (m), Δz_k is the distance between two adjacent streamers (m) and n is the number of streamers mounted on the trap.

3.1.3 Granulometric Data

Using a small core, we collected 10 sediment samples along the study area's beach face (fig. 4). 3 sediment samples were collected on the surf zone seabed of the study areas (fig. 4) at almost 1 m water depth, using a 5 l Van Veen grab. The sediment grain size was determined using the ASTM international standard method (D422-63 and D2217-85) with eight sieves spaced from 8mm to 63μm. Median diameter (D50) and ninety percent diameter (D90) were extracted using geometric graphical measures (Folk & Ward, 1957) and Gradistat software (Blott, S. J. and Pye, 2001). Additionally, granulometric curves were elaborated for CR, CF, and GB sites.

3.1.4 Wave Data

The wave parameters have been downloaded from Copernicus Marine Service Information. In particular, we used data from the product "Mediterranean Sea Waves Analysis and Forecast" (Korres et al., 2023). The variables include offshore significant wave height (H_o), wave period at spectral peak (T_p), and mean direction of the wave from (D_{ir}). We used a 12-hour time series of wave parameters for each day in which we carried out the LST measurements (fig. 7 a. b and c). Only for the GB site, we also considered the significant wave height (H_b), the wave period at spectral peak ($T_{p,br}$) and the mean direction ($D_{ir,br}$) at the breaking point, computed by the Rosario SWAN Wave Model (fig. 7 d) from the i-waveNet project database (https://data.ocean.mt/oceanDataPortal/public/).

3.2 LST bulk formulas

Among the several available approaches, the LST rates for dry mass ($Q_{t,\,mass}$, kg/s) were calculated through three different bulk LST formulas (1), (2) and (3) proposed by CERC (1984), Kamphuis (1991) and Van Rijn (2014), respectively. The Eq. (1) and (2) were selected because they are the most widely used in the literature, while the Eq. (3) formula was chosen because, in addition to being more recent, it was specifically calibrated for beaches with gravel-sized sediments.

$$Q_{t,mass} = 0.03k\rho g^{0.5}(H_b)^2(h_b)^{0.5}sin(2\theta_{br})\left[\frac{\rho_s}{(\rho_s-\rho)}\right] \quad (1)$$

$$Q_{t,mass} = 2.33(T_p)^{1.5}(tan\beta)^{0.75}(H_b)^2(D_{50})^{-0.25}[\sin(2\theta_{br})]^{0.6}\left[\frac{\rho_s}{(\rho_s-\rho)}\right] \quad (2)$$

$$Q_{t,mass} = 0.00018\rho_s g^{0.5}(tan\beta)^{0.4}(H_b)^{3.1}(D_{50})^{-0.6}sin(2\theta_{br}) \quad (3)$$

where ρ is the mass density of seawater (1025 kg/m^3), g is the gravity acceleration (9.81 m/s^2), ρ_s is the mass density of the sediment (2650 kg/m^3), T_p (s) is the wave period at spectral peak, D50 (m) is the median grain size, H_b is the breaking wave height (m), h_b is the water depth at breaking point (m) and θ_{br} is the breaker angle. In formula (2), $tan\beta$ is the slope of the surf zone, whereas, in formula (3), it corresponds to the slope of the surf zone or the beach slope when the beach is sandy or gravelly, respectively. *k* is a dimensionless coefficient relating sand transport to longshore energy flux (0.2 - 1.6, Bodge & Kraus, 1991). We tested four *k* values: the minimum (0.2), the maximum (1.6), the most used in literature (0.39), and the average value (0.77).

The parameters H_b, h_b and θ_{br} were calculated by using equations (4) and (5) proposed by Rattanapitikon and Shibayama (2006) and equation (6) by Larson et al. (2010), respectively. We chose equations (4) and (5) because they provide good accuracy for the cases of $H_o/L_o \leq 0,1$ (Robertson et al., 2013).

$$H_b = (-0.57tan\beta^2 + 0.31tan\beta + 0.58)L_o\left(\frac{H_o}{L_o}\right)^{0.83} \quad (4)$$

$$h_b = (3.86tan\beta^2 - 1.98tan\beta + 0.88)H_o\left(\frac{H_o}{L_o}\right)^{-0.16} \quad (5)$$

$$\theta_{br} = arcsin\left(\sqrt{2\pi}sin\theta_o\sqrt{\frac{h_b}{L_o}}\right) \quad (6)$$

where θ_o is the angle between the offshore wave direction and the perpendicular to the coastline, H_o is offshore significant wave height and L_o is the offshore wavelength that was estimated through the deep-water wave dispersion equation (7).

$$L_o = \frac{g}{2\pi} {T_p}^2 \tag{7}$$

3.3 Numerical model

We used XBeach 2DH numerical model to simulate nearshore and coastal hydrodynamic and morphodynamic processes (e.g. wave propagation, sediment transport, seabed morphological changes) at kilometer and storm time scales (D. Roelvink et al., 2009, 2010). The time-varying wave action balance solved in XBeach 2DH model in surfbeat mode is as follows:

$$\frac{\partial E}{\partial t} + \frac{\partial E C_{g,u}}{\partial s} + \frac{\partial E C_{g,v}}{\partial n} + \frac{\partial E C_{\vartheta}}{\partial \vartheta} = -Sink$$

where E is the wave energy or wave action, C_g is the group velocity, C_ϑ the refraction speed in theta-space and Sink refers to wave breaking and bottom friction effects.

Sediment accretion and erosion are modelled through the depth-averaged advection-diffusion equation (Galappatti & Vreugdenhil, 1985), calculating the difference between the actual depth-averaged sediment concentration and the equilibrium concentration (further details of theoretical background in (D. Roelvink et al., 2009, 2018). This approach allows us to estimate the sediment transport rate and to determine the seabed morphological changes at each time step.

We used the Surfbeat module in the 1.24.6057 Halloween XBeach 2DH model release to resolve the short-wave variations on the wave group scale and the associated long waves. Regarding the wave boundary conditions, we chose the time-varying JONSWAP spectrum with a duration of 1h for a single spectrum and 12h for the whole simulation. Local wind and tidal set-up were not considered in the model set-up.

The sediment transport rate was calculated using the Van Rijn equations (1993). The initial water level (z0) was set to zero, the morphological acceleration factor (morfac) was set to 1, and the simulation time was adapted to the morfac (morfacopt=1). The grain size of the seabed is set using D50 and D90 sediment fractions derived from grain size analysis of seabed samples (see section 3.1.3). The computational domain extends up to 20 m of water depth from the emerged area, corresponding to the input wave parameters' depth (fig. 4) provided by the Copernicus database (see section 3.1.4). To generate the model grid and merge bathymetric and topographic datasets, we used the Deltares Open Earth Toolbox in MATLAB (https://oss.deltares.nl/web/xbeach/tools). We set a grid with variable-size cells in x direction. The cell size was calibrated to find a good compromise between number of cells and computational time. The grid consists of cells with a maximum size of 10 m for CR and GB sites and 5 m for CF site in sectors with water depths greater than closure depth (Hallermeier, 1981). For depths below the wave/seabed interaction depth, the cell size decreases landward from the maximum value (10m for CR and GB sites and 5m for CF site) to the minimum one of 0.5 m. The XBeach 2DH model parameter set of computational domains (e.g. cell corners, cell dimensions, directional limits, directional resolution) is reported in Table S1.

To obtain the best fit between the model result and field data, we performed the models considering the specific characteristics of the study areas (e.g. wave data, grain size, morphology). To do this, we selected two parameter sets related to the sediment transport and morphology modules embedded in the XBeach 2DH software. These parameters were chosen based on their documented influence on LST, as highlighted by several authors (Bugajny et al., 2013; Elsayed & Oumeraci, 2017; Hwang et al., 2024; Satheeshkumar & Balaji, 2021). The sediment transport parameters included *facua*, *bdslpeffmag*, *facsl*, *bdslpeffini*, *reposeangle*, *form*, *lws*, and *turb*, while the morphology parameters included *wetslp*, *morfac*, and *morfacopt* (see Table 1 for description). Moreover, we calibrated the parameter “alfaD50” to improve the sensitivity of the LST formulas to grain size, as indicated in the release note of the software XBeach 2DH model v. 1.24.6057 (tab. 1).

The calibration process involved adjusting each parameter's default values individually to assess its impact on the model’s predictions and identify optimal values that provided the closest match between the model predictions and the field data. We combined these parameters in various configurations to improve the model’s accuracy and achieve the final calibrated setup. Due to the different characteristics of the study areas, we chose different calibrations for GB and CR sites and validated the parametrization of the GB site in the CF site. The list of calibrated parameters and the used values is shown in Table 1. The vegetation module of XBeach 2DH model was used to model the dissipation mechanism of short and long waves caused by seabed vegetation in the GB site. We schematized the vegetation in vertical elements and considered its characteristics (e.g. height from the seabed, stem diameter, density) from literature data (Borg et al., 2005).

To calculate the LST rates, we averaged the values obtained at 11.00 am, 11.30 am, 12.00 am and 12.30 pm in the cell closest to the field measurement point for each site. The time interval 11.00 – 12.30 was chosen because it corresponds with field measurements. Lastly, we calculated the error as the standard deviation between the considered values.

4. Results

4.1 Morphology of the study areas

The CR site is a 3.1 km² wide-open system. The emerged beach is about 1.5 km long in the ENE-WSW direction and 40 m wide from the coastline landward. The maximum elevation value is 5 m, decreasing seaward with an average slope of 1.4°. The slope is 1.7° along the transect that crosses the streamer trap location (transect CTL, fig. 4 a). The submerged sector extends up to 1.8 km from the coastline and reaches 20 m of water depth (fig. 4 a). Based on the wave heights considered for this study, the surf zone reaches depths of about 1.8 m and elongates seaward for 77 m from the coastline with a slope of 1.35°, measured along the transect CTL. From the surf zone to offshore, the seabed gradually deepens with a constant slope, as suggested by the equidistant contours (fig. 4 a).

The CF site is an embayed system that covers an area of 2.2 km². The site is bounded on its northern and southern sides by headlands, which extend 560 m and 290 m seaward and elevate up to 52 m and 3.6 m, respectively. The emerged beach is about 1.7 km long in the NE-SW direction and up to 2.5 m high along its landward boundary. From there, the beach extends 25 m to the coastline with an average slope of about 4°. At the same time, the beach slope reaches 5.1° along the transect CTL (fig. 4 b). The submerged sector is up to 1.1 km long from the coastline and is characterized by depths of up to 17 m. The surf zone elongates 50 m seaward with a slope of 1.44°, measured along the transect CTL (fig. 4 b), and reaches 1.3 m of depth. From the surf zone to offshore, the slope decreases gradually, as indicated by the increase of the mutual distance of the contour lines, locally interrupted by slope breaks (fig. 4 b).

The GB site is an embayed system of 7 km² that consists of an emerged beach trending in the NNW-SSE direction and limited by headlands on both sides. The northern and southern structural highs elongate for 3 km and 2.4 km seaward, respectively, and show a maximum elevation of 60 m and 89 m. The emerging beach is about 900 m long and up to 2 m high (fig. 4 c). It shows a width of 40 m from the coastline landward and an inclination of 1.3° along the transect CTL. The submerged sector extends about 3.5 km from the coastline and up to 30 m in depth (fig. 4 c). The surf zone is 28 m long and reaches a maximum water depth of 1 m with a slope of 1.36°, measured along the transect CTL (fig. 4 c). From the surf zone to offshore, the seabed is characterized by a decreasing slope suggested by the seaward increase of the mutual distance of the contour lines. In the western sector, between 0.5 km to 3 km from the coastline, the seabed shows an irregular morphology with several slope breaks (fig. 4 c).

4.2 Granulometric analysis

Granulometric analysis was performed on sediment samples collected from the surf zone seabed (fig. 4 a, b and c for location) and from the beach face.

Three beach samples collected in the CR site (fig. 4a for location) are defined by D50 values ranging between 0.36 mm and 1.26 mm, with an average value of 0.72 mm (fig. 5a). Whereas the D90 values are from 0.75 mm to 6.37 mm, with an average of 3 mm. The seabed sample (fig. 4a for location) has a D50 value of 6.33 mm and a D90 value of 239.97 mm (fig. 5a).

Three beach and seabed samples were collected in the CF site (fig. 4b for location). Beach samples are characterized by D50 values ranging from 0.19 mm to 0.56 mm, with an average value of 0.42 mm (fig. 5b). D90 values vary from 0.34 mm to 0.93 mm, with an average value of 0.71 mm. The seabed sample yields a D50 value of 0.69 mm and a D90 value of 7.96 mm (fig. 5b).

Four beach and seabed samples were taken at the GB site (fig. 4c for location). Regarding the beach samples, the average value of D50 is 0.26 mm, with a maximum value of 0.34 mm and a minimum of 0.20 mm (fig. 5c). Whereas the D90 averaged 0.44 mm, ranging from 0.38 mm to 0.49 mm. The seabed sample is defined by values of 0.19 mm and 0.40 mm for D50 and D90, respectively (fig. 5c).

4.3 Marine vegetation in the Għadira Bay site

The distribution map of seabed vegetation in the GB site (fig. 6) was obtained by UAV images investigating an area of 1.48 km^2 (see fig. 6 for the seaward limit of the study area). The map shows patchy beds of vegetation that cover an area of 0.8 km^2. Marine vegetation extends from the coastline to 10 m of depth on the GB site's northern and southern sides. In the western sector, it is recognised as starting at least 150 m from the coastline seaward and reaching a maximum depth of 15 m in the central sector.

According to Borg et al. (2005), the vegetation type is *P. oceanica*, characterized by an average leaf width and length of 0.8cm and 45cm, respectively, and a shoot density of 27/0.05 m^2.

4.4 Wave parameters

We used offshore wave parameters (Table S2, fig. 7 a, b and c) derived from the Copernicus database (see section 3.1.4) to estimate the LST rates by XBeach 2DH modelling and bulk formulas. To apply the bulk formulas, we calculated a) L_o and θ_o (tab. 2) using the equations described in section 3.2; b) the wave-breaking parameters (H_b, θ_{br}, h_b in tab. 2) using the mean value of the offshore wave parameters (H_o, D_{ir}, T_p in tab. 2) recorded in the time interval that is the closest to the time of the field LST measurements; c) tanβ, where β is the slope of the surf zone or the beach slope depending on the used formula (see section 3.2). The parameter values used in the bulk formulas are summarized in tab. 2.

For the GB site, we also used wave parameters H_b, D_{ir} and T_p, derived from Rosario SWAN wave model (fig. 7 d) and corresponding with mean values of 0.58 m, 148°N and 9.23 s, respectively. We considered these data to estimate θ_{br} and h_b through equations (6) and (5) described in section 3.2. The obtained values are 88° for the θ_{br} and 1.16 m for h_b.

4.5 LST Rate results

The LST rates were obtained through three methods: field measurements by the streamer trap, bulk formulas, and XBeach 2DH model.

The average values of the LST rate, derived from two field measurements for each site (tab. 3), are $3.69\cdot10^{-03}\pm9.6\cdot10^{-04}$ kg/s in the CR site, $3.19\cdot10^{-03}\pm 4.0\cdot10^{-04}$ kg/s in the CF site and $1.04\cdot10^{-03}\pm 2.6\cdot10^{-04}$ kg/s in the GB site.

The LST rate values, obtained by bulk formulas, were schematised in Table 4. We specify that the CERC formula (1984) result, reported in Table 4, was obtained considering the k value of 0.2. We tested other three k values (see paragraph 3.2 and tab. 5) and chose the formula result derived from the minimum k value of 0.2 because it is the closest to the measured LST rate.

XBeach 2DH calibrated model results are shown in Figure 8. The curves represent the LST rate values along the longshore transect CTL. The modelled LST rates derive from the average of the values obtained at 11.00 am, 11.30 am, 12.00 pm and 12.30 pm in the closest cell to the field measurement point for each site (black point in fig. 8). The average LST rates are $2.93 \cdot 10^{-03} \pm 3.1 \cdot 10^{-04}$ kg/s for the CR site and $5.66 \cdot 10^{-03} \pm 4.7 \cdot 10^{-03}$kg/s for the CF site. At the GB site, we computed the LST rate both considering the presence of *P. oceanica* on the seabed (fig. 8d) and without it (fig. 8c). The average LST rates are $1.95 \cdot 10^{-03} \pm 1.6 \cdot 10^{-03}$ kg/s and 2.9±0.5 kg/s, respectively with/without the marine vegetation.

5. Discussions

As mentioned before, to identify the most accurate method for estimating LST in three different coastal settings located in Malta Island and northern Sicily, we computed the LST rate through three different bulk formulas and XBeach 2DH model and, successively, we compared the predictions of the formulas and model with the value of the field measured LST rate. This section is devoted to comparing and discussing the results of the considered approaches to identify the potential and limitations of each.

5.1 Comparison between bulk formulas' results and observations

LST rate estimations based on the CERC (1984) and Kamphuis (1991) formulas show respectively an overestimation factor of 1857 and 1827 in the CR site, 4825 and 7885 in the CF site, 710 and 3280 in the GB site (considering formulas with H_b value from Rosario database). Despite the results of the Van Rijn formula (2014) representing the lowest values for all study areas, they have an overestimation factor of 435 in the CR site, 3420 in the CF site, 610 in the GB site (considering the formula with H_b value obtained from Rosario database).

The misfit between the value of LST rate, predicted by bulk formulas, and the field measurements was widely documented in previous studies (Bodge & Kraus, 1991; Eversole & Fletcher, 2003; Mil-Homens et al., 2013; Pereira Quadrado & Goulart, 2020; Salem Cherif et al., 2019; Sanil Kumar et al., 2003; Shanas & Sanil Kumar, 2014; Wang et al., 1998; Williams et al., 2008). These researchers focused on studying the parameters that influence the LST rate value to improve the accuracy of the bulk formulas. According to Van Rijn (2003) and Pereira Quadrado & Goulart (2020), the accuracy of the formulas' results depends on the accuracy of the wave parameters, which is related to the method used to calculate them. We tested how the accuracy of the wave parameters influences the LST rate in the GB site. To do this, we used H_b values obtained from the empirical formula Eq. 4 (see paragraph 3.2) and Rosario database. The latter is computed using SWAN wave model that considers the processes of propagation, generation, dissipation and nonlinear wave-wave interactions (Booij et al., 1996). For this reason, the SWAN wave model is considered more accurate than the empirical formula derived from laboratory data (Rattanapitikon & Shibayama, 2006). Our findings highlight that the bulk formula results are up to 200 times lower when we use H_b values derived from the Rosario database than H_b values derived from the empirical formula (fig. 9c). Although using a more accurate wave parameter allowed us to reduce the gap between the field measurement and the bulk formulae results (fig. 9c), these values are still overestimated by a factor of up to 3280 compared to the measured LST rate values. However, a limitation of our study is that the SWAN model data is only available for the GB site. We could not apply this more accurate approach across all three sites, which may have further refined our understanding of the discrepancies observed in LST rate predictions.

The accuracy of the formulas also results from the calibration of key parameters that influence the LST rate (J. D. Rosati, 2005; Wang & Kraus, 1999), such as the wave height and the grain size. Wang et al. (1998) recommended using the CERC formula (1984) in storm conditions where H_s exceed 4 m. The study areas of this research are characterized by low wave conditions with H_s values of about 1 m. Thus, the LST rate values derived from the CERC formula (1984) are overestimated probably because the wave conditions of our sites are different from those recommended by Wang et al. (1998) for the best performance of the CERC formula (1984). Moreover, since it is impossible to acquire measurements with wave heights exceeding 1 m due to the manual installation of the trap and the possibility of its overturning, it is impractical to compare our results under the optimal conditions suggested for the CERC formula. In other areas under low wave conditions, Shanas and Sanil Kumar (2014) obtained overestimated LST rates of factor 1.7 using the CERC formula (1984), whereas Van Rijn (2014) obtained overestimated LST rates of factor 5 and 3 using the CERC (1984) and Kamphuis (1991) formulas, respectively.

Regarding the grain size, a different weight was assigned to it by bulk formulas through an exponential function. Kamphuis (1991) empirically determined the exponent of D50 and found that the LST rate is inversely proportional to $D50^{0.25}$. This result indicates that sediment transport depends only slightly on grain size. Conversely, other studies highlight a stronger dependence of the LST rate on the grain size (Mil-Homens et al., 2013;

Tomasicchio et al., 2013; Van Rijn, 2014). Among these, Van Rijn (2014) assigned to D50 an exponent through numerical models and found that LST rate is inversely proportional to $D50^{0.6}$. Our results show that LST rates predicted by the Van Rijn formula (2014) are closer to the measured data than the Kamphuis formula (1991) in all study areas (fig 9 a-b-c). This finding confirms the strong dependence of the LST rate on the grain size. Although the Van Rijn formula (2014) is more accurate than the Kamphuis formula (1991), the results overestimate those measured in the field. The discrepancy is probably due to the wave conditions (θ_o =30°, H_s = 3m, T_p = 8 s) used by Van Rijn (2014) to calibrate the D50, which are not representative of the average conditions of our study areas.

The D50 value is not considered in the CERC formula (1984). However, the formula includes the parameter k, which is linked to several factors, such as the grain size and breaker type (J. Rosati et al., 2002; Wang & Kraus, 1999). Several authors tried to calibrate k to improve the LST rate estimated by the CERC formula (Bodge & Kraus, 1991; del Valle et al., 1993; Eversole & Fletcher, 2003; Schoonees & Theron, 1993; Van Wellen et al., 2000). In our study, we tested four *k* values in the range proposed by Bodge and Kraus (1991): the minimum (0.2), the maximum (1.6), the most used in literature (0.39), and the average value (0.77). The obtained LST rate values are overestimated in our study areas (see tab. 5), both with fine sand (GB site), coarse sand (CF site) and gravel (CR site). Despite the use of different k values, previous studies highlighted that CERC formula (1984) results generally overpredict the LST rate up to 3000% (Bayram et al., 2007; Bodge & Kraus, 1991; Eversole & Fletcher, 2003; Pereira Quadrado & Goulart, 2020; Salem Cherif et al., 2019; Shanas & Sanil Kumar, 2014; Wang et al., 1998, 2002). Thus, it would be appropriate to improve the calibration of k and not use a single value of k for all longshore transport conditions.

Another factor that controls the LST rate is the presence of marine vegetation on the seabed. The vegetation limits the erosion of sediments, dissipating the energy of the currents on the bottom and reducing the shear stress at the sediment-water interface (Le Hir et al., 2007; Widdows & Brinsley, 2002). The two actions cause, in turn, a decrease in the LST rate. This condition occurs in the GB site, where the seabed is covered by *P. oceanica*. Therefore, the overestimation of the LST rates is partly due to neglecting marine vegetation as a parameter of the bulk formulas.

5.2 Comparison between XBeach 2DH model results and observations

XBeach 2DH model results indicate a good agreement between modelled values and field measurements. The average modelled and measured LST rates are, respectively, 0.003 kg/s and 0.004 kg/s in the CR site, 0.006 kg/s and 0.003 kg/s in the CF site, 0.002 kg/s and 0.001 kg/s in the GB site.

Previous studies suggest calibrating the model based on specific characteristics (e.g. wave data, grain size, morphology) of the study area and to fine-tune the model result until the output fits with field data (Bergillos et al., 2017; Elsayed & Oumeraci, 2017; Garzon et al., 2022; Hwang et al., 2024; Jin et al., 2021; McCall et al., 2010; Satheeshkumar & Balaji, 2021; Simmons et al., 2019; Simmons & Splinter, 2022). We calibrated the model based on parameters (see paragraph 3.3) that are considered the most influential on the LST rate (Bugajny et al., 2013; Elsayed & Oumeraci, 2017; Hwang et al., 2024; Satheeshkumar & Balaji, 2021; XBeach User Manual v. 1.24.6057).

The model results of the GB site are in good agreement with those obtained from field observations, showing an overestimate of factor 1.9. The model's good performance in the GB site is due to the calibration and the possibility of including the presence of *P. oceanica* on the seabed in the modelling. We tested the model both with and without the "vegetation module" to verify the influence of marine vegetation on the LST rate. Our results show that the LST rate significantly reduces from 2.9 kg/s to 0.002 kg/s when the model includes the marine vegetation, fitting the field measurement of the LST rate (0.001 kg/s). Moreover, this finding confirms that vegetation represents a crucial factor in controlling the LST rate, according to Widdows & Brinsley (2002) and Le Hir et al. (2007).

The calibration values applied to the GB site were successfully validated in the CF site, where the model result overestimates by a factor of 1.8 the field measurement. The calibration showed good performance because both the GB and CF sites have similar characteristics in terms of morphology (embayed system) and grain size (fine/coarse sand). Conversely, the parametrization used for the GB site provides a bad result in the CR site, overestimating a factor of 8 the field measurement. This result is probably due to the characteristics of the CR site, which is an open system with a gravelly beach. Therefore, different values of the parameters were chosen for the calibration of the CR site (see tab. 1). The modelling provides a good result, underestimating the field value by a factor of 0.5.

Despite the D50 of the surf zone at the CR site being coarser than the recommended range for the XBeach 2DH model, the model performs well. Moreover, the modelling value for the CR site (0.003 kg/s) shows a better fitting with the field measurement (0.004 kg/s) compared to that calculated (1.74 kg/s) by the Van Rijn formula (2014), which is commonly used in literature for gravelly beaches.

Additionally, it must be pointed out that other sources of discrepancy between modelling values and observations may also be partly found in the error of the field measurement method used to capture the sediment. The trap is susceptible to oversampling due to initial stirring linked to trap placement and undersampling because the instrumentation represents an obstacle to the sediment moving on the sea bottom. Moreover, the gap between the trap bags does not allow the capture of sediment transported throughout the entire water column. Future studies will focus on improving the quality of measured LST by improving sediment capture methods and performing measurements under variable wave conditions to understand and address these sources of error better.

6. Conclusions

This research assesses the predictive capacity of three of the most commonly used bulk formulas (CERC formula, 1984; Kamphuis formula, 1991 and Van Rijn formula, 2014) and the XBeach 2DH model (Roelvink et al., 2009) for estimating the LST rate in three different coastal settings located in Malta Island (Għadira Bay) and northern Sicily (Cefalù and Campofelice di Roccella sites). For each site, we have analysed the wave parameters (H_o, T_p, D_{ir}, H_b, $T_{p,br}$, $D_{ir,br}$), the grain size of the beach and seabed, the coastal type (open or embayed system), the seabed morphology and the presence of marine vegetation. Moreover, we have estimated the field LST rates and compared the field measurement to the results of applying both formulas and model.

Our finding highlights that the XBeach 2DH model is more accurate than bulk formulas in all the studied sites. Although previous studies have attempted to improve the bulk formulas by calibrating the parameters that control the LST rate, there is still a misfit between predictions and observations. Our results indicate overestimation factors of the CERC formula (1984) ranging from 710 to 4825, Kamphuis formula (1991) ranging from 1827 to 7885, and Van Rijn formula (2014) ranging from 435 to 3420. This deviation may be due to several reasons, among these: a) not considering the 3D-morphological features of the emerged area (open and embayed system) and the seabed; b) the use of coefficients (k in the CERC formula (1984), the exponents of D50 in the Kamphuis formula (1991) and Van Rijn formula (2014)) that have been calibrated based on boundary conditions (e.g. wave height, period, theta, grain size, breaker type) that are not representative of different world regions; c) the neglect of the vegetation on the seabed.

Conversely, the XBeach 2DH model results fit the field measurements, showing an overestimate of a factor of 1.9 in the GB site and 1.8 in the CF site and an underestimate of 0.5 in the CR site. The XBeach 2DH model is the most accurate methodology for predicting the LST rate because the modelling considers the specific characteristics of the study area that influence the LST rate (e.g. wave parameters, grain size and seabed/emerged morphology, presence of marine vegetation).

To obtain the best performance of the XBeach 2DH model, we recommend using the closest wave data to the coastline and extending the model grid seaward until the point corresponding with the wave data location. Moreover, we suggest calibrating the sediment transport parameters (e.g. facua, bdslpeffmag, facsl, bdslpeffini, reposeangle, form, lws, turb) and morphology parameters (e.g. wetslp, morfac, morfacopt) that are considered the most influent on the LST by several authors (Bugajny et al., 2013; Elsayed & Oumeraci, 2017; Hwang et al., 2024; Satheeshkumar & Balaji, 2021) and add the parameter “alfaD50” to the calibration set as indicated in the release note of the software XBeach 2DH v. 1.24.6057.

The good performance of the model in the GB and CF sites demonstrates that the calibration process used in this study can be applied successfully in embayed systems characterized by fine/coarse sandy beaches. Moreover, results obtained in the CR site indicate that the model also performs well in sites characterized by gravelly beaches, highlighting its adaptability to a broader range of environmental conditions than that tested and recommended for the XBeach 2DH model.

References

Bailard, J. A. (1981). An energetics total load sediment transport model for a plane sloping beach. *Journal of Geophysical Research: Oceans*, *86*(C11), 10938–10954. https://doi.org/https://doi.org/10.1029/JC086iC11p10938

Barbariol, F., Davison, S., Falcieri, F. M., Ferretti, R., Ricchi, A., Sclavo, M., & Benetazzo, A. (2021). Wind Waves in the Mediterranean Sea: An ERA5 Reanalysis Wind-Based Climatology. *Frontiers in Marine Science*, *8*(November), 1–23. https://doi.org/10.3389/fmars.2021.760614

Bayram, A., Larson, M., & Hanson, H. (2007). A new formula for the total longshore sediment transport rate. *Coastal Engineering*, *54*(9), 700–710. https://doi.org/10.1016/j.coastaleng.2007.04.001

Bergillos, R. J., Masselink, G., & Ortega-Sánchez, M. (2017). Coupling cross-shore and longshore sediment transport to model storm response along a mixed sand-gravel coast under varying wave directions. *Coastal Engineering*, *129*(July), 93–104. https://doi.org/10.1016/j.coastaleng.2017.09.009

Blott, S. J. and Pye, K. (2001). GRADISTAT: a grain size distribution and statistics package for the analysis of unconsolidated sediments. *Earth Surf. Proc. Land.*, *26*, 1237–1248.

Bodge, K. R., & Kraus, N. C. (1991). Critical examination of longshore transport rate magnitude. *Coastal Sediments*, 139–155.

Booij, N., Holthuijsen, L. H., & Ris, R. C. (1996). The "Swan" Wave Model for Shallow Water. In *Coastal Engineering* (pp. 668–676). https://doi.org/10.1061/9780784402429.053

Borg, J. A., Attrill, M. J., Rowden, A. A., Schembri, P. J., & Jones, M. B. (2005). Architectural characteristics of two bed types of the seagrass Posidonia oceanica over different spatial scales. *Estuarine, Coastal and Shelf Science*, *62*(4), 667–678. https://doi.org/10.1016/j.ecss.2004.10.003

Bugajny, N., Furmańczyk, K., Dudzińska-Nowak, J., & Paplińska-Swerpel, B. (2013). Modelling morphological changes of beach and dune induced by storm on the Southern Baltic coast using XBeach (case study: Dziwnow Spit). *Journal of Coastal Research*, *65*(January), 672–677. https://doi.org/10.2112/si65-114.1

Caloiero, T., Aristodemo, F., & Ferraro, D. A. (2022). Annual and seasonal trend detection of significant wave height, energy period and wave power in the Mediterranean Sea. *Ocean Engineering*, *243*(October 2021), 110322. https://doi.org/10.1016/j.oceaneng.2021.110322

Coastal Engineering Research Center, (US). (1984). *Shore protection manual* (Vols. 1–2). Department of the Army, Waterways Experiment Station, Corps of Engineers, Coastal Engineering Research Center.

Cartier, A., & Héquette, A. (2015). Vertical distribution of longshore sediment transport on barred macrotidal beaches, northern France. *Continental Shelf Research*, *93*, 1–16. https://doi.org/10.1016/j.csr.2014.11.009

Dabees, M., & Kamphuis, J. W. (1998). ONELINE, a numerical model for shoreline change. *Proceedings of the Coastal Engineering Conference*, *3*, 2668–2681. https://doi.org/10.1061/9780784404119.202

Dally, W. R., & Dean, R. G. (1984). Suspended Sediment Transport and Beach Profile Evolution. *Journal of Waterway, Port, Coastal, and Ocean Engineering*, *110*(1), 15–33. https://doi.org/10.1061/(asce)0733-950x(1984)110:1(15)

Dehouck, A., Dupuis, H., & Sénéchal, N. (2009). Pocket beach hydrodynamics: The example of four macrotidal beaches, Brittany, France. *Marine Geology*, *266*(1–4), 1–17. https://doi.org/10.1016/j.margeo.2009.07.008

del Valle, R., Medina, R., & Losada, M. A. (1993). Dependence of coefficient K on grain size. *Journal of Waterway, Port, Coastal, and Ocean Engineering*, *119*(5), 568–574.

DHI. (2005). MIKE 21/3 Flow Model FM Hydrodynamic and Transport Module Scientific Documentation. In *DHI Group Horshølm*.

Dolique, F., & Anthony, E. J. (2005). Short-term profile changes of sandy pocket beaches affected by amazon-derived mud, Cayenne, French Guiana. *Journal of Coastal Research*, *21*(6), 1195–1202. https://doi.org/10.2112/04-0297.1

Drago, A. F., Azzopardi, J., Gauci, A., Bruschi, A., R, T., & Bruschi, A. (2013). Assessing the offshore wave energy potential for the Maltese islands. *ISE Annual Conference*, *March*.

Elsayed, S. M., & Oumeraci, H. (2017). Effect of beach slope and grain-stabilization on coastal sediment transport: An attempt to overcome the erosion overestimation by

XBeach. *Coastal Engineering*, *121*(December 2016), 179–196. https://doi.org/10.1016/j.coastaleng.2016.12.009

Eversole, D., & Fletcher, C. H. (2003). Longshore sediment transport rates on a reef-fronted beach: Field data and empirical models Kaanapali Beach, Hawaii. *Journal of Coastal Research*, *19*(3), 649–663.

Folk, R. L., & Ward, W. (1957). Brazos river bar: a study in the significance of grain size parameters. *Journal of Sedimentary Petrology*, *27(1)*, 3–26.

Galappatti, G., & Vreugdenhil, C. B. (1985). A depth-integrated model for suspended sediment transport. *Journal of Hydraulic Research*, *23*(4), 359–377. https://doi.org/10.1080/00221688509499345

Galdies, C. (2011). *The Climate of Malta: statistics, trends and analysis 1951-2010* (Issue August 2011).

Garzon, J. L., Ferreira, Ó., & Plomaritis, T. A. (2022). Modeling of Coastal Erosion in Exposed and Groin-Protected Steep Beaches. *Journal of Waterway, Port, Coastal, and Ocean Engineering*, *148*(6), 1–16. https://doi.org/10.1061/(asce)ww.1943-5460.0000719

Gatt, P. (2021). Embayment morphometrics, granulometry and carbonate mineralogy of sandy beaches in the Maltese Islands. *Marine Geology*, *432*(June 2020), 106394. https://doi.org/10.1016/j.margeo.2020.106394

Gessler, D., Hall, B., Spasojevic, M., Holly, F., Pourtaheri, H., & Raphelt, N. (1999). Application of 3D mobile bed, hydrodynamic model. *Journal of Hydraulic Engineering*, *125*(7), 737–749.

González, M., Medina, R., Gonzalez-Ondina, J., Osorio, A., Méndez, F. J., & García, E. (2007). An integrated coastal modeling system for analyzing beach processes and beach restoration projects, SMC. *Computers and Geosciences*, *33*(7), 916–931. https://doi.org/10.1016/j.cageo.2006.12.005

Hallermeier, R. (1981). A profile zonation for seasonal sand beaches from wave climate. *Coastal Eng.*, *4*, 253–277.

Hanson, H. (1989). Genesis: A Generalized Shoreline Change Numerical Model. *Journal of Coastal Research*, *5*(1), 1–27. http://www.jstor.org/stable/4297483

Hedegaard, I. B., Deigaard, R., & Fredsøe, J. (1991). Onshore/offshore sediment transport and morphological modelling of coastal profiles. *Coastal Sediments*, 643–657.

Hwang, B., Do, K., & Chang, S. (2024). Morphological Changes in Storm Hinnamnor and the Numerical Modeling of Overwash. *Journal of Marine Science and Engineering*, *12*(1). https://doi.org/10.3390/jmse12010196

Hydraulics, W. (1994). UNIBEST, A software suite for the simulation of sediment transport processes and related morphodynamics of beach profiles and coastline evolution, Programme manual. *WL|Delft Hydraulics, Delft, The Netherlands*.

Jin, H., Do, K., Shin, S., & Cox, D. (2021). Process-based model prediction of coastal dune erosion through parametric calibration. *Journal of Marine Science and Engineering*, *9*(6). https://doi.org/10.3390/jmse9060635

Kamphuis, J. W. (1991). Alongshore sediment transport rate distribution. *Journal of Waterway, Port, Coastal, and Ocean Engineering*, *117*(6), 624–640.

King, E. V., Conley, D. C., Masselink, G., Leonardi, N., McCarroll, R. J., Scott, T., & Valiente, N. G. (2021). Wave, Tide and Topographical Controls on Headland Sand Bypassing. *Journal of Geophysical Research: Oceans*, *126*(8). https://doi.org/10.1029/2020JC017053

Korres, G., Oikonomou, C., Denaxa, D., & Sotiropoulou, M. (2023). *Mediterranean Sea Waves Analysis and Forecast (Copernicus Marine Service MED-Waves, MEDWAM4 system) (Version 1) [Data set]*. Copernicus Monitoring Environment Marine Service (CMEMS). https://doi.org/https://doi.org/10.25423/CMCC/MEDSEA_ANALYSISFORECAST_WAV_006_017_MEDWAM4

Kraus, N. C. (1987). *Rates in the Surf Zone Measurements of Sediment Transport Rate*. *3*(2), 139–152.

Larson, M., Hoan, L. X., & Hanson, H. (2010). Direct Formula to Compute Wave Height and Angle at Incipient Breaking. *Journal of Waterway, Port, Coastal, and Ocean Engineering*, *136*(2), 119–122. https://doi.org/10.1061/(asce)ww.1943-5460.0000030

Le Hir, P., Monbet, Y., & Orvain, F. (2007). Sediment erodability in sediment transport modelling: Can we account for biota effects? *Continental Shelf Research*, *27*(8), 1116–1142. https://doi.org/10.1016/j.csr.2005.11.016

Lesser, G. R., Roelvink, J. A., van Kester, J. A. T. M., & Stelling, G. S. (2004). Development and validation of a three-dimensional morphological model. *Coastal Engineering*, *51*(8–9), 883–915. https://doi.org/10.1016/j.coastaleng.2004.07.014

Masselink, G., Russell, P., Turner, I., & Blenkinsopp, C. (2009). Net sediment transport and morphological change in the swash zone of a high-energy sandy beach from swash event to tidal cycle time scales. *Marine Geology*, *267*(1–2), 18–35. https://doi.org/10.1016/j.margeo.2009.09.003

McCall, R. T., Van Thiel de Vries, J. S. M., Plant, N. G., Van Dongeren, A. R., Roelvink, J. A., Thompson, D. M., & Reniers, A. J. H. M. (2010). Two-dimensional time dependent hurricane overwash and erosion modeling at Santa Rosa Island. *Coastal Engineering*, *57*(7), 668–683. https://doi.org/10.1016/j.coastaleng.2010.02.006

Mil-Homens, J., Ranasinghe, R., van Thiel de Vries, J. S. M., & Stive, M. J. F. (2013). Re-evaluation and improvement of three commonly used bulk longshore sediment transport formulas. *Coastal Engineering*, *75*, 29–39. https://doi.org/10.1016/j.coastaleng.2013.01.004

Pereira Quadrado, G., & Goulart, E. S. (2020). Longshore sediment transport: predicting rates in dissipative sandy beaches at southern Brazil. *SN Applied Sciences*, *2*(6), 23–33. https://doi.org/10.1007/s42452-020-03223-x

Rattanapitikon, W., & Shibayama, T. (2006). Breaking wave formulas for breaking depth and orbital to phase velocity ratio. *Coastal Engineering Journal*, *48*(4), 395–416. https://doi.org/10.1142/S0578563406001489

REGIONE-SICILIANA. (2020). *Piano Regionale Contro l'Erosione Costiera (PRCEC)*.

Robertson, B., Hall, K., Zytner, R., & NISTOR, I. (2013). BREAKING WAVES: REVIEW OF CHARACTERISTIC RELATIONSHIPS. *Coastal Engineering Journal*, *55*(1), 1350002. https://doi.org/10.1142/S0578563413500022

Roelvink, D., McCall, R., Mehvar, S., Nederhoff, K., & Dastgheib, A. (2018). Improving predictions of swash dynamics in XBeach: The role of groupiness and incident-band runup. *Coastal Engineering*, *134*(February 2017), 103–123. https://doi.org/https://doi.org/10.1016/j.coastaleng.2017.07.004

Roelvink, D., Reniers, A., Van Dongeren, A. P., Van Thiel de Vries, J., Lescinski, J., & McCall, R. (2010). XBeach model description and manual. *Unesco-IHE Institute for Water Education, Deltares and Delft University of Tecnhology. Report June*, *21*, 2010.

Roelvink, D., Reniers, A., van Dongeren, A., van Thiel de Vries, J., McCall, R., & Lescinski, J. (2009). Modelling storm impacts on beaches, dunes and barrier islands. *Coastal Engineering*, *56*(11–12), 1133–1152. https://doi.org/10.1016/j.coastaleng.2009.08.006

Roelvink, J. A., & Stive, M. F. J. (1989). Bar-generating cross-shore flow mechanisms on a beach. In *Journal of Geophysical Research* (Vol. 94, Issue C4, pp. 4785–4800). https://doi.org/10.1029/JC094iC04p04785

Rosati, J. D. (2005). Concepts in sediment budgets. *Journal of Coastal Research*, *21*(2), 307–322. https://doi.org/10.2112/02-475A.1

Rosati, J., Walton, T. L., & Bodge, K. (2002). Longshore sediment transport. In *Coastal engineering manual, Part III-2*. Army Corps of Engineers, Washington, DC (engineer manual 1110-2-1100 edition).

Salem Cherif, Y., Mezouar, K., Guerfi, M., Sallaye, M., & Dahmani, A. E. A. (2019). Nearshore hydrodynamics and sediment transport processes along the sandy coast of Boumerdes, Algeria. *Arabian Journal of Geosciences*, *12*(24). https://doi.org/10.1007/s12517-019-4981-0

Samaras, A. G., & Koutitas, C. G. (2014). Comparison of three longshore sediment transport rate formulae in shoreline evolution modeling near stream mouths. *Ocean Engineering*, *92*, 255–266. https://doi.org/10.1016/j.oceaneng.2014.10.005

Sanil Kumar, V., Anand, N. M., Chandramohan, P., & Naik, G. N. (2003). Longshore sediment transport rate - Measurement and estimation, central west coast of India. *Coastal Engineering*, *48*(2), 95–109. https://doi.org/10.1016/S0378-3839(02)00172-2

Satheeshkumar, J., & Balaji, R. (2021). Field Measurement and Modeling of Sediment Transport along a Sandy Pocket Beach, Central West Coast of India. *Journal of*

Waterway, Port, Coastal, and Ocean Engineering, *147*(6), 5021014. https://doi.org/10.1061/(ASCE)WW.1943-5460.0000678

Schoonees, J. S., & Theron, A. K. (1993). Review of the field-data base for longshore sediment transport. *Coastal Engineering*, *19*(1–2), 1–25. https://doi.org/10.1016/0378-3839(93)90017-3

Scott Wilson Kirkpatrick and Co. Ltd. (2003). *Malta Significant Wave Height Study: Main Report*. *December*.

Shanas, P. R., & Sanil Kumar, V. (2014). Coastal processes and longshore sediment transport along Kundapura coast, central west coast of India. *Geomorphology*, *214*, 436–451. https://doi.org/10.1016/j.geomorph.2014.02.027

Simmons, J. A., & Splinter, K. D. (2022). A multi-model ensemble approach to coastal storm erosion prediction. *Environmental Modelling and Software*, *150*. https://doi.org/10.1016/j.envsoft.2022.105356

Simmons, J. A., Splinter, K. D., Harley, M. D., & Turner, I. L. (2019). Calibration data requirements for modelling subaerial beach storm erosion. *Coastal Engineering*, *152*(November 2018), 103507. https://doi.org/10.1016/j.coastaleng.2019.103507

Soukissian, T., Karathanasi, F., Axaopoulos, P., Voukouvalas, E., & Kotroni, V. (2018). Offshore wind climate analysis and variability in the Mediterranean Sea. *International Journal of Climatology*, *38*(1), 384–402. https://doi.org/10.1002/joc.5182

Sperati, S., Alessandrini, S., D'Amico, F., Cheng, W., Rozoff, C. M., Bonanno, R., Lacavalla, M., Aiello, M., Airoldi, D., Amaranto, A., Decimi, G., & Vergata, M. A. (2024). A new Wind Atlas to support the expansion of the Italian wind power fleet. *Wind Energy*, *27*(3), 298–316. https://doi.org/10.1002/we.2890

Tassi, P., Benson, T., Delinares, M., Fontaine, J., Huybrechts, N., Kopmann, R., Pavan, S., Pham, C. T., Taccone, F., & Walther, R. (2023). GAIA - a unified framework for sediment transport and bed evolution in rivers, coastal seas and transitional waters in the TELEMAC-MASCARET modelling system. *Environmental Modelling and Software*, *159*(September 2022), 105544. https://doi.org/10.1016/j.envsoft.2022.105544

Tomasicchio, G. R., D'Alessandro, F., Barbaro, G., & Malara, G. (2013). General longshore transport model. *Coastal Engineering*, *71*, 28–36. https://doi.org/10.1016/j.coastaleng.2012.07.004

Van Rijn, L. C. (1993). *Principles of sediment transport in rivers, estuaries and coastal seas*. International Institute for Infrastructural, Hydraulic, and Environmental Engineering, Delft, The Netherlands.

Van Rijn, L. C. (2003). LONGSHORE SAND TRANSPORT Leo C. van Rijn 1. *28th ICCE, Cardiff, UK*, 1–13.

Van Rijn, L. C. (2014). A simple general expression for longshore transport of sand, gravel and shingle. *Coastal Engineering*, *90*, 23–39. https://doi.org/10.1016/j.coastaleng.2014.04.008

Van Wellen, E., Chadwick, A. J., & Mason, T. (2000). A review and assessment of longshore sediment transport equations for coarse-grained beaches. *Coastal Engineering*, *40*(3), 243–275. https://doi.org/10.1016/S0378-3839(00)00031-4

Walton, T. L., Bruno, R. O., Walton Jr, T. L., & Bruno, R. O. (1989). Longshore transport at a detached breakwater, phase II. *Journal of Coastal Research*, *1982*, 679–691.

Wang, P., & Kraus, N. C. (1999). Longshore sediment transport rate measured by short-term impoundment. *Journal of Waterway, Port, Coastal, and Ocean Engineering*, *125*(3), 118–126.

Wang, P., Kraus, N. C., & Davis, R. A. (1998). Total longshore sediment transport rate in the surf zone: Field measurements and empirical predictions. *Journal of Coastal Research*, *14*(1), 269–282.

Wang, P., Smith, E. R., & Ebersole, B. A. (2002). Large-scale laboratory measurements of longshore sediment transport under spilling and plunging breakers. *Journal of Coastal Research*, *18*(1), 118–135.

Widdows, J., & Brinsley, M. (2002). Impact of biotic and abiotic processes on sediment dynamics and the consequences to the structure and functioning of the intertidal zone. *Journal of Sea Research*, *48*(2), 143–156. https://doi.org/10.1016/S1385-1101(02)00148-X

Williams, J. J., Esteves, L. S., & Lisniowski, M. A. (2008). Towards improving the prediction of longshore sediment transport. *IAHS-AISH Publication*, *325*, 599–606.

XBeach manual: Release XBeach 1.24.6057 Halloween. (2023). *Https://Xbeach.Readthedocs.Io/En/Latest/Index.Html*.

Captions

Table 1. *Calibrated parameters and used values for Għadira Bay (GB), Cefalù (CF) and Campofelice di Roccella (CR) sites.*

Table 2. *Parameter values used in the bulk formulas.*

Table 3. *LST values derived from field measurements by streamer trap. Values 1 and 2 were obtained by measurements in the time interval, respectively, between 11.30 – 11.40 a.m. and 12.10 and 12.20 on 27th July 2023 at the Campofelice di Roccella site, on 24th January 2024 at the Għadira Bay site and 2nd April 2024 at the Cefalù site.*

Table 4. *LST rate computed by bulk formulas in each study area. In the Għadira Bay site, bulk formulas were tested using H_b derived from empirical formula (H_bEF) and Rosario database (H_bRD).*

Table 5. *LST rate computed using the CERC formula (1984), varying k value in each study areas. In the Għadira Bay site, bulk formulas were tested using H_b derived from empirical formula (H_bEF) and Rosario database (H_bRD).*

Table S1. *Main XBeach parameter set.*

Table S2. *The time series of offshore wave parameters downloaded from the Copernicus database for Għadira Bay, Campofelice di Roccella and Cefalù sites.*

Figure 1. *(a) Geographic locations of the study areas: (b) northern Sicily, featuring the sites of (c) Campofelice di Roccella and (d) Cefalù; and (e) Għadira Bay (GB) on Malta Island.*

Figure 2. *Wave rose of annual mean significant wave height and direction at the sites a) Campofelice di Roccella, b) Cefalù and c) Għadira Bay, between 12 a.m. on 1 January 1993 and 11 p.m. on 31 December 2023. The red points in the maps indicate the offshore points where wave parameters have been downloaded from the Copernicus Marine Service Information.*

Figure 3. *(a) Streamer trap used to measure field LST rate. b) An example of an acquisition survey at the Cefalù Site was performed on 02 April 2024, with a significant offshore wave height of 0.6m, direction 297°N, and period of 8 s.*

Figure 4. *Topobathymetric maps of a) Campofelice di Roccella, b) Cefalù and c) Għadira Bay. The stars indicate the position of LST rate measurements using the streamer trap and surf zone seabed sampling. The black dots indicate the position of the collected beach samples. The red rectangles indicate the limits of XBeach 2DH models' computational domain. The dashed orange lines AA' (a and d), BB' (b and e) and CC' (c and f) show the bathymetric profiles crossing the streamer trap location (transect CTL; see section 4.1).*

Figure 5. *Grain size curves of seabed (SB) and beach samples collected in a) Campofelice di Roccella site (CR1, CR2, CR3), b) Cefalù site (CF1, CF2, CF3) and c) Għadira Bay site (GB1, GB2, GB3, GB4). See fig. 4 for sample locations.*

Figure 6. *Map of Posidonia oceanica distribution on the Għadira Bay seabed. The green cells indicate the presence of marine vegetation. The solid black line represents the coastline and the dotted red line represents the seaward limit of the investigated area. The blue lines are the isobaths of 10m and 15 m.*

Figure 7. *Offshore wave height (blue line) and direction (red line) data downloaded from Copernicus Marine Service Information for a) the Campofelice di Roccella site, b) the Cefalù site and c) the Għadira Bay site. In d) wave height (blue line) and direction (red line) data at the breaking point computed by the Rosario SWAN Wave Model from the i-waveNet project database for the Għadira Bay site.*

Figure. 8. *Graphs of LST rate derived from calibrated XBeach 2DH model at a) Campofelice di Roccella site, b) Cefalù site, c) and d) Għadira Bay site. The graphs show the LST rate computed at the time 11:00 a.m. (orange dotted line), 11:30 a.m. (blue dotted line), 12:00 p.m. (green dotted line) and 12:30 p.m. (purple dotted line) along the longshore transect crossing the trap location (black dot).*

Figure 9. *LST rate values measured by streamer trap and computed by bulk formulas and XBeach 2DH model at a) Campofelice di Roccella site, b) Cefalù site and c) Għadira Bay*

site. In the latter site, the performance of the bulk formula was tested using H_b derived from the empirical formula (H_bEF) and Rosario database (H_bRD), while the performance of the XBeach 2DH model was evaluated not considering the presence of marine vegetation (NCVeg) and considering it (CVeg).

Tables

Table 1.

Parameter and Description	Default value	Range value	Tested value	Used value for GB and CF sites	Used value for CR site
facua - Calibration factor time averaged flows due to wave skewness and asymmetry	0.175	0.0 - 1.0	0.02, 0.1, 0.35, 0.175	0.35	0.35
alfaD50 - Calibration coefficient for grain size term	0.4	0-1	0 0.25, 0.4, 0.75, 1	0.25	0.4
bdslpeffmag - Modify the magnitude of the sediment transport based on the bed slope	roelvink_total	none, roelvink_total, roelvink_bed, soulsby_total, soulsby_bed	None, roelvink_bed, soulsby_bed, soulsby_total, roelvink_total	soulsby_bed	soulsby_bed
facsl - Factor bedslope effect	1.6	0-1.6	0, 0.15, 0.8, 1.6	1.6	1.6
bdslpeffini - Modify the critical shields parameter based on the bed slope	none	none, total, bed	total, bed, none	total	total
reposeangle - Angle of internal friction	30	0-45	30, 35, 40	30	35
form - Equilibrium sediment concentration formulation	vanthiel_vanrijn	soulsby_vanrijn, vanthiel_vanrij, vanrijn1993	soulsby_vanrijn, vanthiel_vanrij, vanrijn1993	Vanrijn1993	Vanrijn1993
lws - Switch to enable long wave stirring	1	0-1	0, 1	0	0
turb - Switch to include short wave turbulence	wave_averaged	none, wave_averaged, bore_averaged	none, wave_averaged, bore_averaged	none	none
wetslp - Critical avalanching slope under water	0.15	0.1-1	0.15, 0.1, 0.5, 1	0.15	0.15
morfac - Morphological acceleration factor	1	0.0 - 1000.0	0, 1	1	1
morfacopt - Switch to adjusting output times for morfac	1	0-1	0, 1	1	1

Table 2.

Parameters for bulk formulas									
Site	**H_0 (m)**	**D_{ir} (°N)**	**T_p (s)**	**L_o (m)**	**θ_o**	**H_b (m)**	**θ_{br} (degree)**	**h_b (m)**	**tanβ**
Għadira Bay	1.44	27.64	8.39	109.90	32.00	1.76	11.34	2.41	0.02
Cefalù	0.72	296.96	8.39	109.90	28.04	0.99	7.47	1.34	0.03
Campofelice di Roccella	1.04	326.81	7.63	90.82	8.19	1.31	2.86	1.78	0.02 (surf zone) 0.03 (beach)

Table 3.

Field measured LST rate (kg/s)		
Site	**Value 1**	**Value 2**
Għadira Bay	$9.08 \cdot 10^{-04}$	$1.16 \cdot 10^{-03}$
Campofelice di Roccella	$4.17 \cdot 10^{-03}$	$3.21 \cdot 10^{-03}$
Cefalù	$2.99 \cdot 10^{-03}$	$3.40 \cdot 10^{-03}$

Table 4.

LST rate (kg/s) computed by bulk formulas				
Formula	**Għadira Bay**		**Campofelice di Roccella**	**Cefalù**
	(H_bEF)	(H_bRD)		
CERC (1984)	60.84	0.71	7.43	9.65
Kamphuis (1991)	80.25	3.28	7.31	15.77
Van Rijn (2014)	123.98	0.61	1.74	6.84

Table 5.

LST rate (kg/s) derived from CERC formula (1984)				
Site \ **k**	**0.20**	**0.39**	**0.77**	**1.60**
Ghadira Bay (H_bEF)	60.84	118.63	234.22	486.69
Ghadira Bay (H_bRD)	0.71	1.38	2.73	5.67
Campofelice di Roccella	7.43	14.49	28.62	59.46
Cefalù	9.65	18.82	37.15	77.19

Table S1.

Parameter	Description	Value		
		Għadira Bay	Campofelice di Roccella	Cefalù
nx	Number of computational cell corners in cross-shore direction	651	493	397
ny	Number of computational cell corners in longshore direction	119	166	196
dx_{max}/dx_{min}	Dimensions of cell in cross-shore direction	10 - 0.5m	10 – 0.5m	5 - 0.5m
dy	Dimensions of cell in longshore direction	15m	10m	10m
thetamin	Lower directional limit	145	231	213
thetamax	Higher directional limit	275	296	296
dtheta	Directional resolution	10	10	10
dtheta_s	Directional resolution in case of stationary refraction	10	10	10

Table S2.

Ghadira Bay			
H_0 (m)	T_p (s)	D_{ir} (°N)	dd-MM-yyyy HH:mm
1.30	7.63	332.74	24/01/2024 02:00
1.24	7.63	333.29	24/01/2024 03:00
1.18	7.63	333.97	24/01/2024 04:00
1.11	7.63	334.61	24/01/2024 05:00
1.13	7.63	335.78	24/01/2024 06:00
1.05	6.93	338.37	24/01/2024 07:00
1.03	6.93	342.29	24/01/2024 08:00
1.07	6.93	350.75	24/01/2024 09:00
1.18	7.63	6.60	24/01/2024 10:00
1.35	8.39	23.27	24/01/2024 11:00
1.52	8.39	32.00	24/01/2024 12:00
1.65	9.23	35.33	24/01/2024 13:00
Campofelice di Roccella			
1.37	7.63	330.78	27/07/2023 02:00
1.34	7.63	330.38	27/07/2023 03:00
1.31	7.63	329.96	27/07/2023 04:00
1.27	7.63	329.40	27/07/2023 05:00
1.40	8.39	328.94	27/07/2023 06:00
1.33	8.39	328.72	27/07/2023 07:00
1.27	8.39	328.56	27/07/2023 08:00
1.21	8.39	328.29	27/07/2023 09:00
1.15	8.39	327.89	27/07/2023 10:00
1.09	7.63	327.40	27/07/2023 11:00
1.04	7.63	326.77	27/07/2023 12:00
0.99	7.63	326.26	27/07/2023 13:00
Cefalù			
0.55	8.39	296.45	02/04/2024 02:00
0.56	8.39	295.39	02/04/2024 03:00
0.54	8.39	293.79	02/04/2024 04:00
0.53	7.63	291.30	02/04/2024 05:00
0.53	7.63	287.07	02/04/2024 06:00
0.54	7.63	276.83	02/04/2024 07:00
0.53	8.39	277.17	02/04/2024 08:00
0.51	8.39	283.73	02/04/2024 09:00
0.51	8.39	289.72	02/04/2024 10:00
0.52	8.39	294.33	02/04/2024 11:00
0.60	8.39	297.43	02/04/2024 12:00
0.59	8.39	299.13	02/04/2024 13:00

Figures

Figure 1.

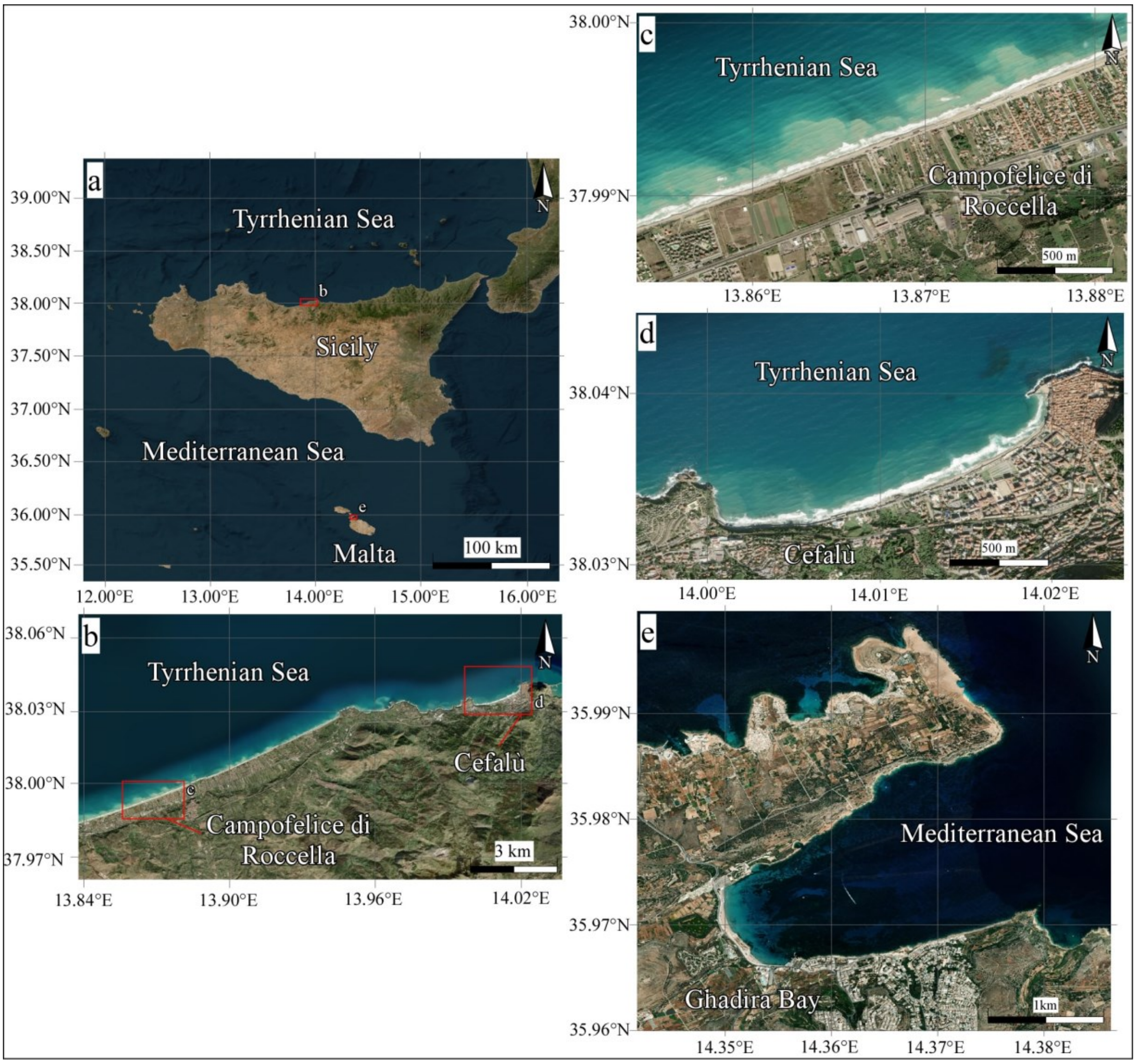

Figure 2.

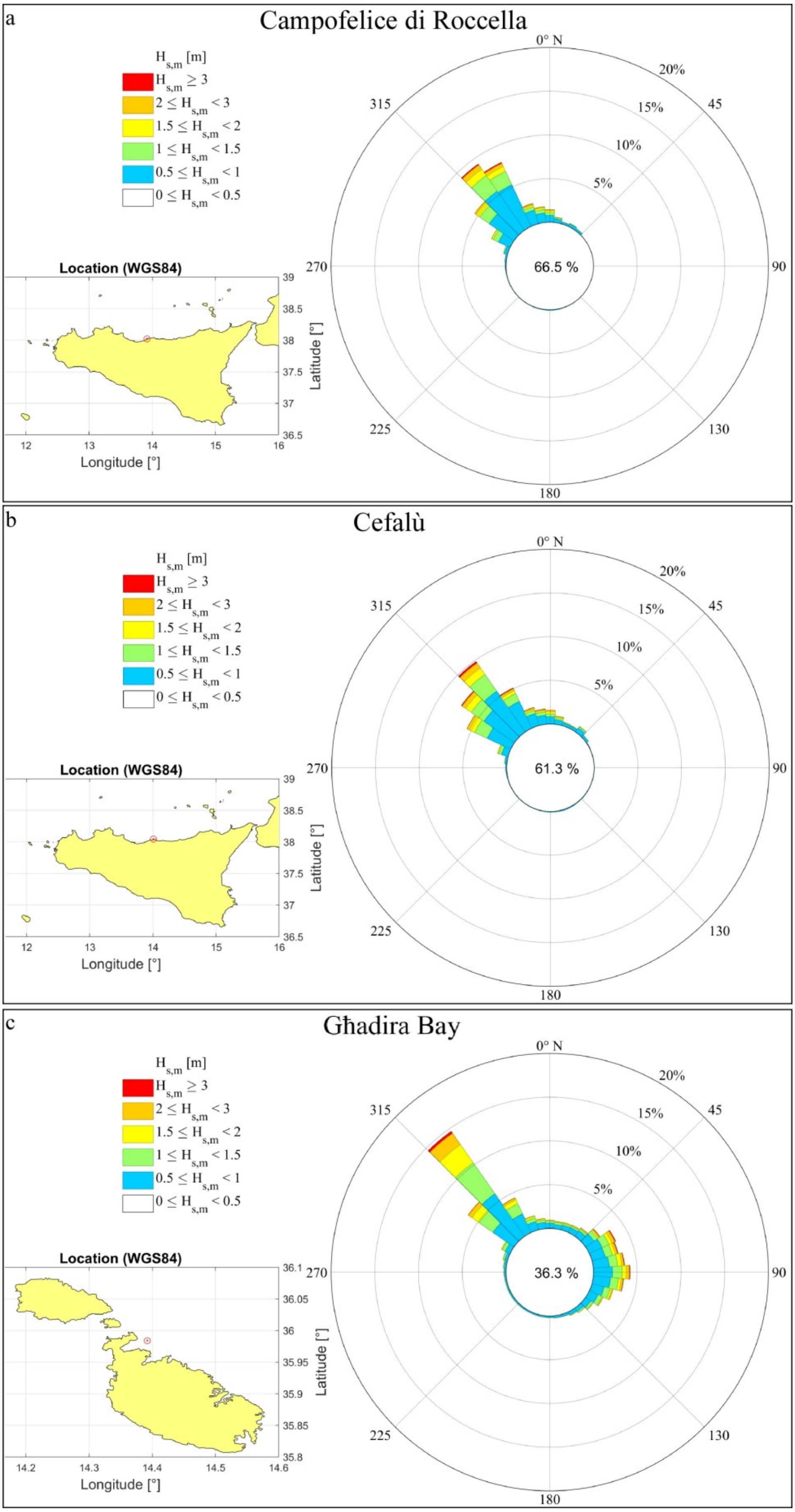

a
Campofelice di Roccella
$H_{s,m}$ [m]
$H_{s,m} \geq 3$
$2 \leq H_{s,m} < 3$
$1.5 \leq H_{s,m} < 2$
$1 \leq H_{s,m} < 1.5$
$0.5 \leq H_{s,m} < 1$
$0 \leq H_{s,m} < 0.5$
Location (WGS84)
Longitude [°]
Latitude [°]
0° N
20%
15%
10%
5%
315
45
270
90
225
130
180
66.5 %
b
Cefalù
61.3 %
c
Għadira Bay
36.3 %

Figure 3.

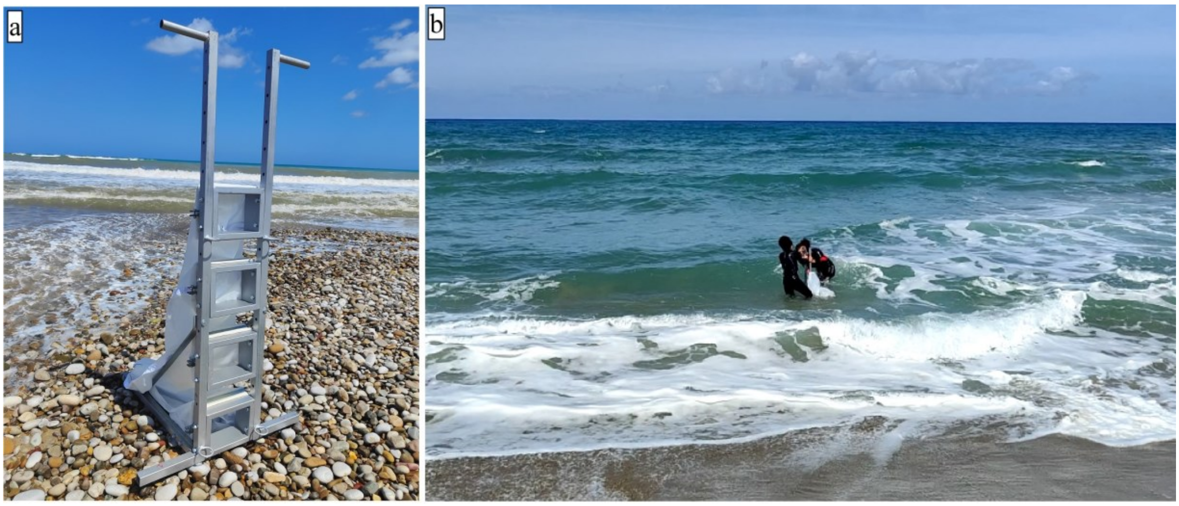

Figure 4.

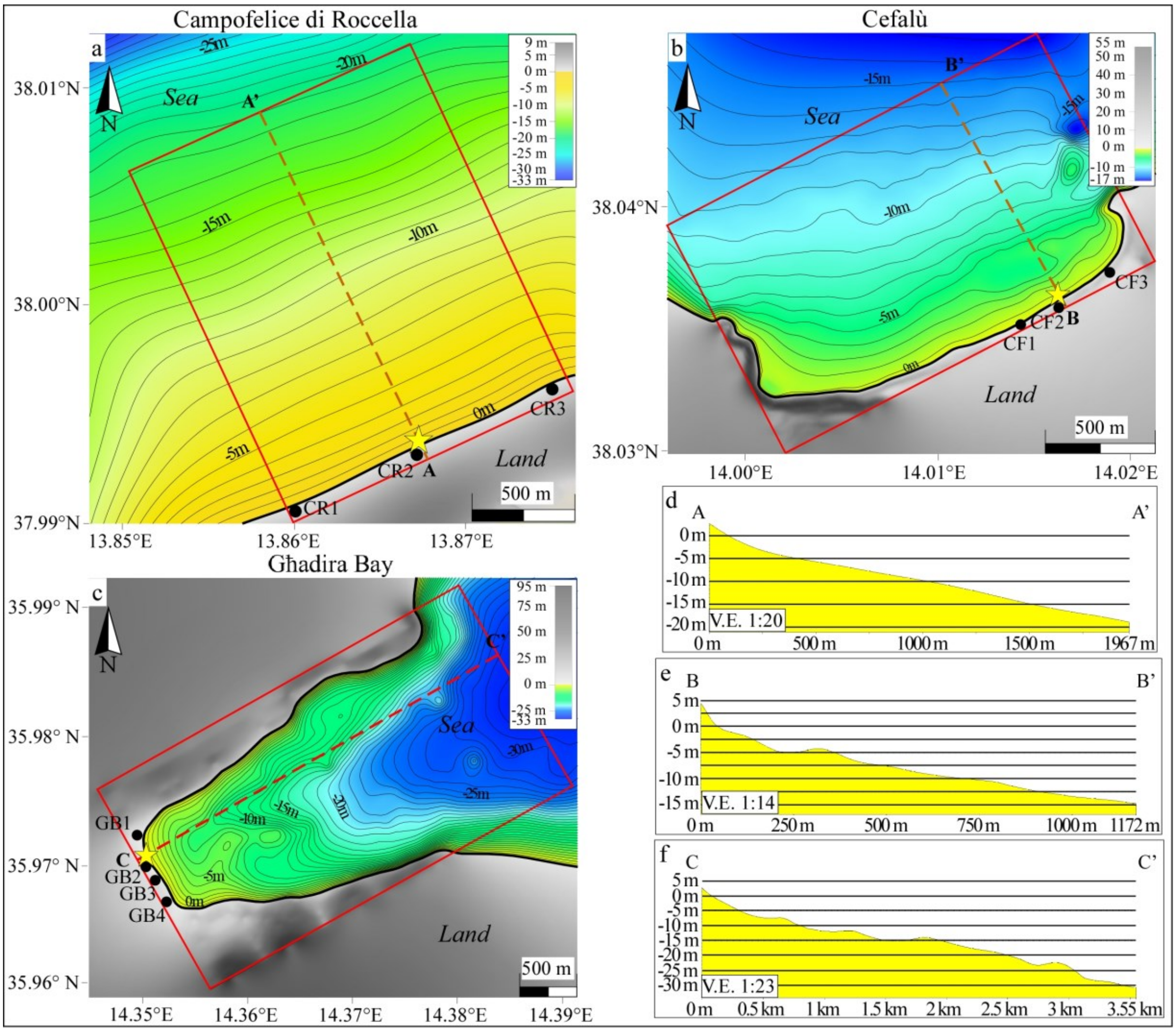

Campofelice di Roccella
Cefalù
Għadira Bay
a
b
c
d
e
f
Sea
Land
N
A
A'
B
B'
C
C'
CR1
CR2
CR3
CF1
CF2
CF3
GB1
GB2
GB3
GB4
500 m
V.E. 1:20
V.E. 1:14
V.E. 1:23
38.01°N
38.00°N
37.99°N
13.85°E
13.86°E
13.87°E
38.04°N
38.03°N
14.00°E
14.01°E
14.02°E
35.99° N
35.98° N
35.97° N
35.96° N
14.35°E
14.36°E
14.37°E
14.38°E
14.39°E
0m
500m
1000m
1500m
1967m
250m
750m
1172m
0.5km
1km
1.5km
2km
2.5km
3km
3.55km

Figure 5.

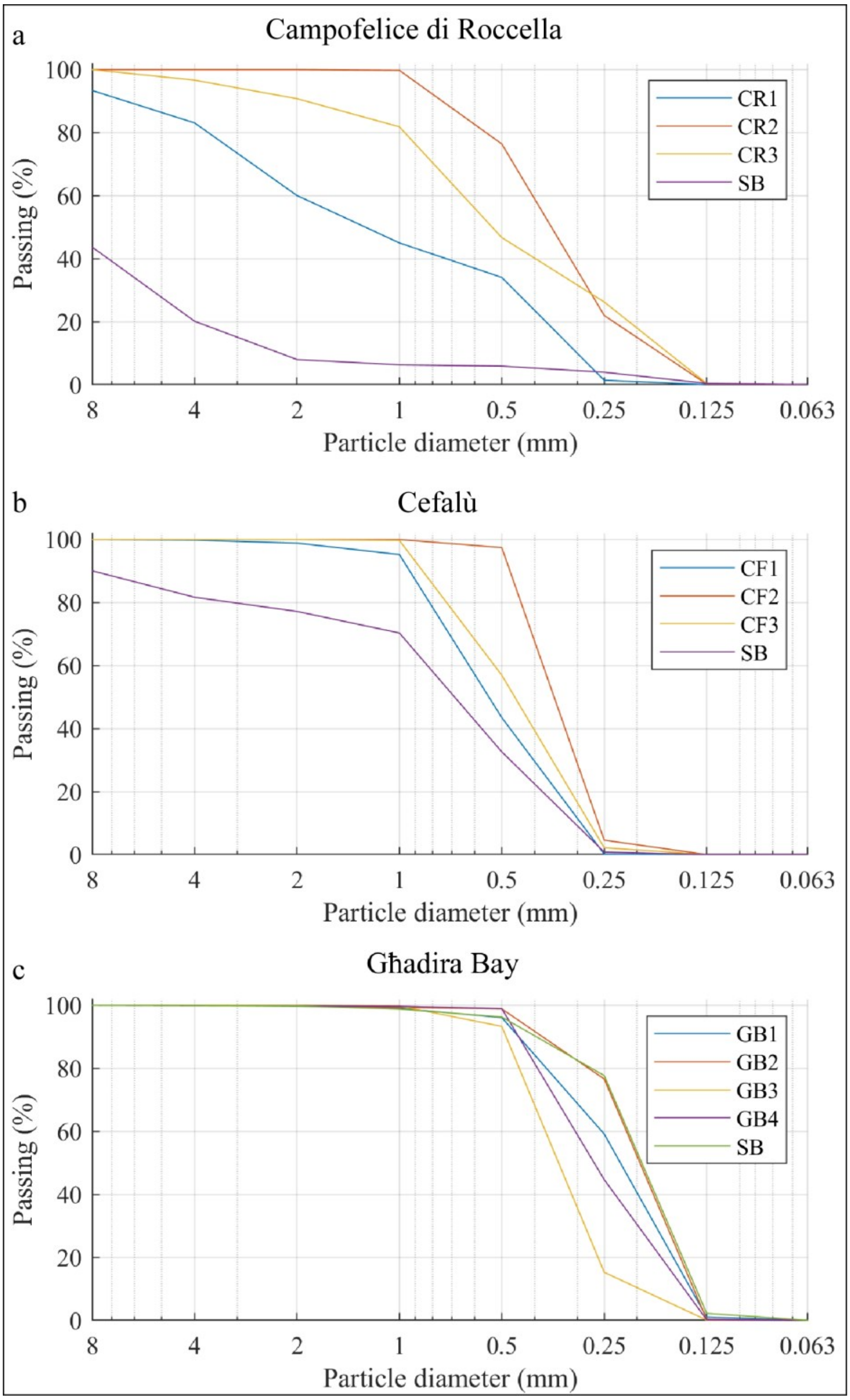
a
Campofelice di Roccella
100
80
60
40
20
0
Passing (%)
8
4
2
1
0.5
0.25
0.125
0.063
Particle diameter (mm)
CR1
CR2
CR3
SB
b
Cefalù
Passing (%)
Particle diameter (mm)
CF1
CF2
CF3
SB
c
Għadira Bay
Passing (%)
Particle diameter (mm)
GB1
GB2
GB3
GB4
SB

Figure 6.

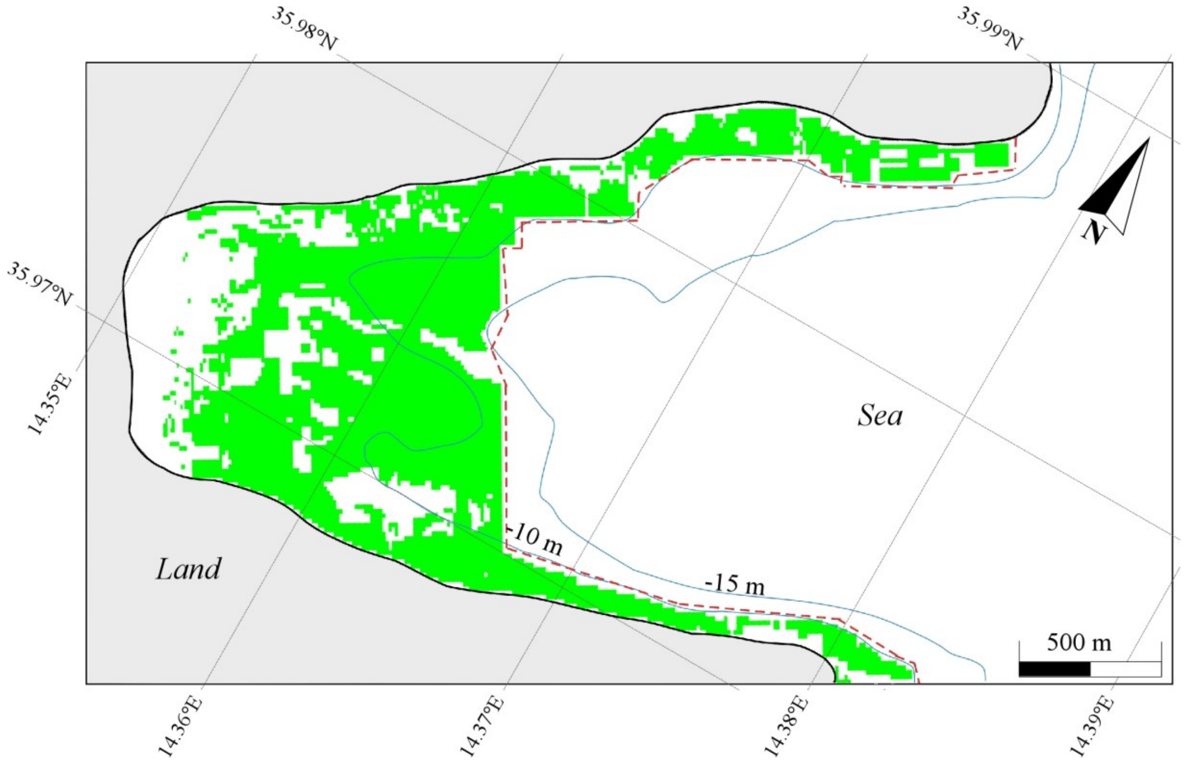

35.98°N
35.99°N
35.97°N
14.35°E
N
Sea
-10 m
-15 m
Land
500 m
14.36°E
14.37°E
14.38°E
14.39°E

Figure 7.

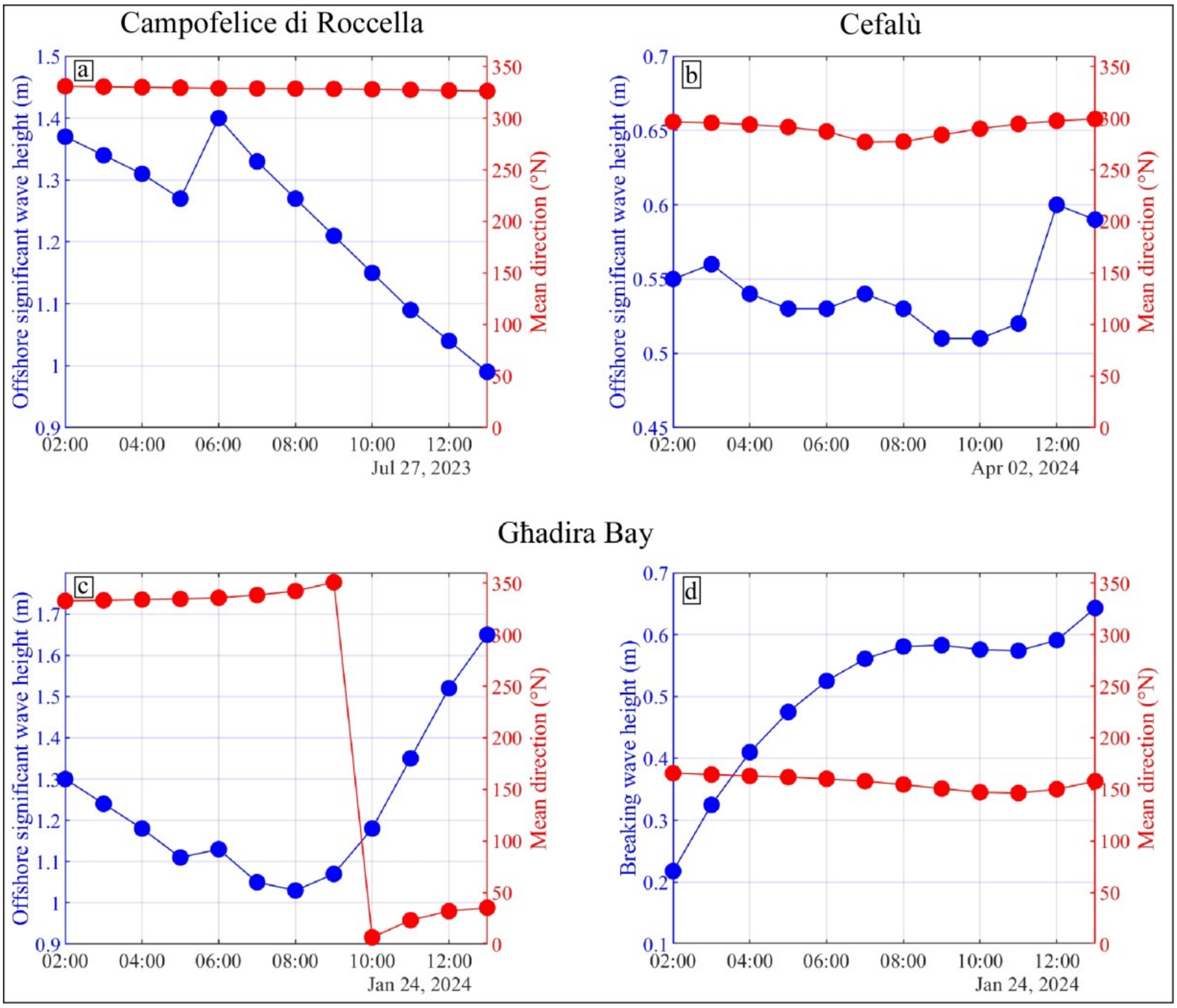

Campofelice di Roccella
Cefalù
Għadira Bay
a
b
c
d
Offshore significant wave height (m)
Breaking wave height (m)
Mean direction (°N)
Jul 27, 2023
Apr 02, 2024
Jan 24, 2024
Jan 24, 2024

Figure 8.

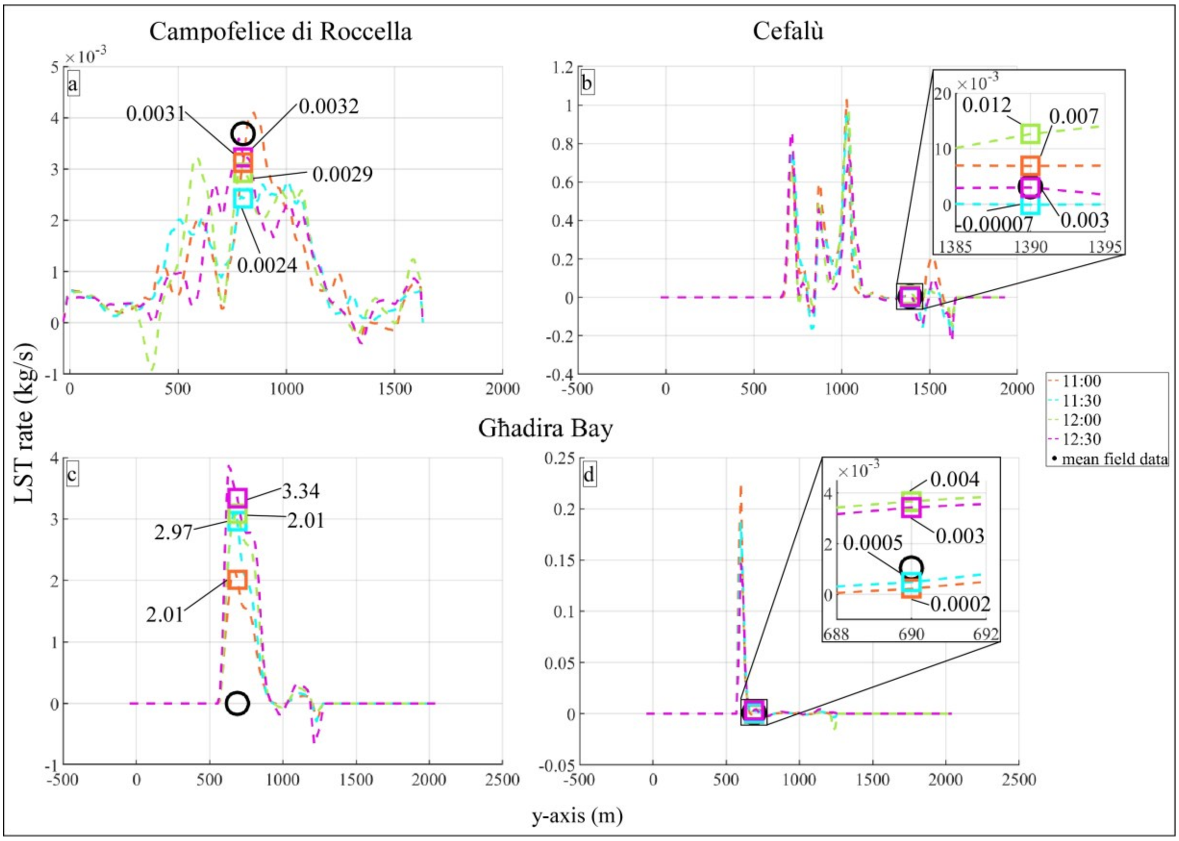

Campofelice di Roccella
Cefalù
Għadira Bay
a
b
c
d
0.0031
0.0032
0.0029
0.0024
0.012
0.007
-0.00007
0.003
3.34
2.97
2.01
2.01
0.004
0.003
0.0005
0.0002
LST rate (kg/s)
y-axis (m)
11:00
11:30
12:00
12:30
mean field data

Figure 9.

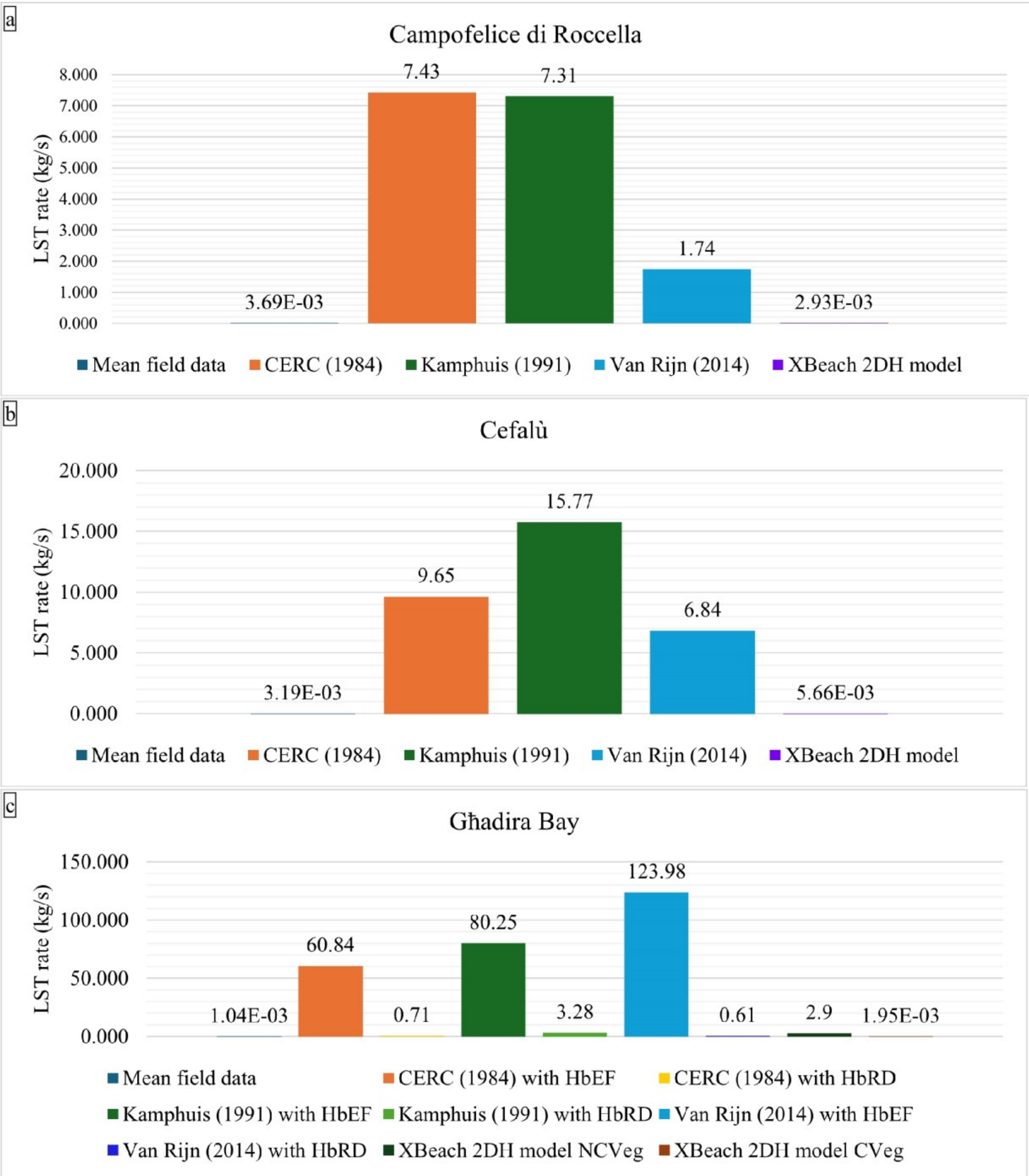
a
Campofelice di Roccella
LST rate (kg/s)
8.000
7.000
6.000
5.000
4.000
3.000
2.000
1.000
0.000
3.69E-03
7.43
7.31
1.74
2.93E-03
Mean field data
CERC (1984)
Kamphuis (1991)
Van Rijn (2014)
XBeach 2DH model
b
Cefalù
LST rate (kg/s)
20.000
15.000
10.000
5.000
0.000
3.19E-03
9.65
15.77
6.84
5.66E-03
Mean field data
CERC (1984)
Kamphuis (1991)
Van Rijn (2014)
XBeach 2DH model
c
Għadira Bay
LST rate (kg/s)
150.000
100.000
50.000
0.000
1.04E-03
60.84
0.71
80.25
3.28
123.98
0.61
2.9
1.95E-03
Mean field data
CERC (1984) with HbEF
CERC (1984) with HbRD
Kamphuis (1991) with HbEF
Kamphuis (1991) with HbRD
Van Rijn (2014) with HbEF
Van Rijn (2014) with HbRD
XBeach 2DH model NCVeg
XBeach 2DH model CVeg

CHAPTER 2

Coastal Vulnerability Index to erosion

NOTE: This chapter is a work-in-progress scientific paper in collaboration with Faraci C., Corradino M., Colica E. and Pepe F.

Abstract

Coastal areas face increasing erosion, flooding, and environmental degradation risks due to changing climate and human development. This study proposes a Coastal Vulnerability Index (CVI) tailored to assess erosion vulnerability at the beach scale. The CVI integrates four sub-indices: Morphological Characteristics (MC), Shoreline Displacement (SD), Longshore Sediment Transport (LST), and Wave Height (WH). Data from aerial surveys, bathymetric maps, and wave climate records were utilized, while sediment transport was modelled using XBeach 2DH. The study was conducted at Għadira Bay, a pocket beach located in northeastern Malta. Results revealed low vulnerability in most sections of the bay, except for one section, which showed moderate vulnerability, driven primarily by higher sediment transport rates. The proposed CVI, which incorporates natural and physical factors such as marine vegetation and headlands, offers an enhanced approach to quantifying coastal erosion risk. This research provides essential tools for local governments to improve coastal management strategies and mitigate risks associated with erosion.

Keywords: Coastal Vulnerability Index, Coastal Erosion, Longshore Sediment Transport, XBeach 2DH numerical mode, Coastal Management

1. Introduction

Coastal areas are vulnerable to several factors, including flooding, erosion, subsidence and changes in meteorological and oceanographic conditions. The potential for environmental and economic damage is exacerbated by coastal development, resulting in already degraded coastal habitats (i.e., marshes, beaches, and islands) being more vulnerable to losses (Doukakis, 2005; Kleini et al., 2016). Local governments often lack access to scientific information to plan coastal defence systems. Providing local governments with information on the scale of the area they manage (Bourne et al., 2016) and enabling close collaboration between scientists and municipal staff (Wamsler et al., 2014) are essential to achieving practical implementation of coastal management.

Coastal vulnerability assessment can contribute to planning measures to counteract erosion by identifying, quantifying and classifying vulnerability. Methodologies for coastal vulnerability assessment can be classified into (Ramieri et al., 2011): indicator-based or index-based methods, GIS-based decision support systems, dynamic modelling approaches and visualisation tools. Among these, index-based methods are widely used for their simplicity in integrating multiple variables into a single Coastal Vulnerability Index (CVI). CVI allows the definition of coastal section vulnerability by attributing it to a rank of vulnerability, ranging from low to very high (Gornitz et al., 1991). A literature review indicates several CVI assessment methods exist (Balica et al., 2012; Gornitz, 1990; McLaughlin et al., 2002; Mcleod et al., 2010; Ramieri et al., 2011). Some approaches focus on analysing vulnerability components (e.g., geological, physical, and socio-economic) to provide a CVI at various time and spatial scales (Rocha et al., 2020; Yin et al., 2012). Other methods use numerical models to investigate the hydrodynamic and morphodynamic impacts of storm events at the scale of a single beach (Oliveira et al., 2021; Serafim et al., 2019). However, these methods often do not incorporate the analysis of sedimentary dynamics in the submerged coastal sector, which is influenced by biotic and abiotic factors (e.g. marine vegetation, waves and currents). Integrating data from studies on the factors and processes influencing sediment dynamics in coastal and marine environments is essential for comprehending coastal vulnerability to erosion.

This research proposes a CVI to erosion that refers to the scale of a single beach. The proposed approach relies on quantitative/qualitative assessment and numerical approximations of physical and geological indexes that drive sediment input/output into coastal and marine environments, governing beach evolution. Sub-indexes include Morphological Characteristics (MC), Shoreline displacement (SD), Longshore Sediment Transport (LST) and Wave Height (WH). The proposed CVI is tested on Għadira Bay (GB), a pocket beach located in the north-eastern sector of Malta Island.

Research outcomes provide an instrument to facilitate informed decision-making for planning strategies related to population protection, infrastructure preservation, cultural heritage conservation, and maintaining natural habitats in coastal areas.

2. Study areas

Għadira Bay is a pocket beach, trending in the NNW-SSE and limited by headlands on both sides (fig. 1). The emerged beach is about 900 m long and up to 2 m high and limited landward by a seawall (Buttò et al. *submitted*). The seabed of the surf zone, 28 m long and 1 m deep at most is characterised by a decreasing slope seaward. In the western sector, between 0.5 km and 3 km from the coastline, the seabed shows an irregular morphology with several interruptions in slope (Buttò et al. *submitted*).

The seabed is characterized by the presence of *Posidonia oceanica* (Borg et al., 2005). The distribution of P. oceanica consists of patchy beds located on the northern and southern sides from the coastline to 10 m in depth. In the western sector, it is recognised starting at least 150 m from the coastline (Buttò et al. *submitted*).

The coastal climate of Għadira Bay is influenced by air pressure systems emerging from the Atlantic and surrounding land areas. Storm activity primarily impacts the area in autumn and winter, resulting from the interaction between low-pressure systems and warm, moist Mediterranean air (Galdies, 2011). The wave climate shows a marked seasonal energy variation, with the highest energy levels occurring from November to April (Drago et al., 2013). The average yearly significant wave height is 1.22 m, rising to 1.92 m during winter (Drago et al., 2013).

3. Materials and methods

The methodology selected for the vulnerability assessment is based on calculating sub-indexes that concern all those characteristics that can make the coastline sensitive to erosive dynamics. For this reason, the chosen sub-indexes are related to the MC of the beaches (both the emerged and submerged part), the SD of the coastline, the LST rate and the WH. When combined, these sub-indexes allow for calculating a final overall CVI.

The methodology proposed involves four phases of work for its development (tab. 1). An extensive dataset comprising aerial photographs, digital elevation models (DEMs), GPS data, wave data (e.g., significant wave height, wave period and wave direction) and grain-size data is collected in the first phase. During the second phase, we split the beach under study into sections based on their width and the presence of rigid structures (naturals and anthropogenic). The third phase is used to calculate the proposed sub-indexes. Finally, the CVI is calculated during the fourth step, and vulnerability maps are realised.

3.1 Data collection

Different datasets were used to estimate the parameters involved in calculating each sub-index. Bathymetric maps from 0 to approximately 20 m of depth were acquired in 2023 using a 235 kHz Ohmex SonarMite V5 single beam echo-sounder mounted on a small inflatable craft. These data were integrated with Topcon Hyper HR GNSS data collected in a depth range from 0 to approximately 1.5 m (Buttò et al. *submitted*). Aerial photogrammetric data of GB's emerged and submerged coastal area was acquired in October

2019 and November 2023 by an unmanned aerial vehicle (UAV) Mavic 3 (Buttò et al. *submitted*). The photogrammetric data were used to obtain DEMs, orthophoto and the map of Posidonia oceanica distribution in the area extending from the coastline to 10 meters of depth (Buttò et al. *submitted*). Satellite images of May 2021 and April 2013 were obtained from Google Earth Pro. Aerial photo of 1998 was provided by Malta Planning Authority. Median diameter (D50) and ninety percent diameter (D90) were obtained by Buttò et al., (*submitted*), analysing sediment samples collected on the surf zone seabed. Wave parameters have been downloaded from Copernicus Marine Service Information. We used data from the product "Mediterranean Sea Waves Analysis and Forecast" (Korres, G., Oikonomou, C., Denaxa, D., & Sotiropoulou, 2023). The variables include offshore significant wave height (H_o, average height, trough to crest, of the one-third highest sea surface waves), wave period (T_p) and the mean direction of the wave from (D_{ir}). We analysed a dataset covering the period from 1st January 1993 to 31st December 2023 to identify the most frequent and maximum wave parameters.

3.2 Coastal Vulnerability sub-index

For calculating vulnerability sub-indexes, we selected methods with careful consideration given to their feasibility of estimating the individual parameters involved, particularly concerning field measurements. The methodologies to calculate each sub-index are summarized below.

3.2.1 Morphological Characteristics sub-index

MC sub-index includes the characteristics of the coastal area (both emerged and submerged parts) representing a natural defence system against erosion. Five variables were considered to determine the MC sub-index: slope of the submerged beach (%), beach width (m), length of headlands (m), presence of marine vegetation and presence of dune systems.

The parameter "length of headlands" refers to the extent of promontories from the coastline. Headlands can disrupt longshore sediment exchange when their length exceeds the distance at which the depth of closure is reached in the nearshore zone. To classify the vulnerability associated with the length of the promontory, the value associated with maximum vulnerability was chosen as the mean distance, measured along the measurement sections, from the shoreline to the isobath of the depth of closure. Other vulnerability classes were defined using intervals of the 25th percentile of the mean distance value (tab. 2).

Regarding width and slope measurements, the landward limit of the emerged beach was defined by either a morphological feature (e.g., a dune) or a human structure (e.g., a coastal wall). In contrast, the seaward limit was represented by the wet/dry line (Boak & Turner, 2005). Additionally, the wet/dry line served as the landward limit for measuring the slope of the submerged beach, with the seaward limit determined by the bathymetry corresponding to the depth of closure. The latter is calculated using the Hallermeier formula (2), which is based on storm wave characteristics (Hallermeier, 1981):

$$h_c = 2.28H_o - 68.5\left(\frac{H_o^2}{gT_p^2}\right) \tag{1}$$

where H_o is the offshore significant wave height (average height, trough to crest, of the one-third highest sea surface waves), T_p is wave period, and g is the acceleration of gravity, while the correction coefficients proposed in the equations result from a numerical Froude relation describing the sediment suspension.

The overall MC sub-index was determined as the average of the vulnerability values of the considered variables. Following the methodology proposed by (Gornitz et al., 1991), the measured variable values were classified into five classes (tab. 2).

3.2.2 Shoreline Displacement sub-index

The SD sub-index is an indicator of the health of a coastline. The SD analysis was based on estimating the coastline's horizontal variation rate (vo) over different time intervals. We used shorelines from the past 2, 4, 10 and 25 years, obtained by orthophotos and aerial photo (fig. 2), to estimate v_o (m/y) over the time intervals Most Recent (MR), Short Term (ST), Middle Term (MT) and Long Term (LT), respectively. The vulnerability classification was done by dividing v_o into five classes (Gornitz et al., 1991). The trends calculated for the various time intervals were combined into a weighted average, with the increasing weight assigned to shorter time intervals (tab. 3). The decision to place greater emphasis on short-term trends reflects the need to analyse the current vulnerability of the coastline, along with the higher accuracy of data from more recent shorelines.

3.2.3 Longshore Sediment Transport sub-index

The LST sub-index is introduced to consider LST as a key mechanism for moving sediments along the coastline. LST occurs when waves approach the shore at an angle different from 90°, with maximum effectiveness observed at a 45° wave incidence (Siegle

& Asp, 2007). No significant morphological changes occur as long as the amount of sediment entering and leaving a specific coastal section remains balanced. Erosion or accretion of the coast happens when there is a transport imbalance. A positive gradient, which indicates an increase in sediment transport, leads to shoreline retreat, while a negative gradient causes a reduction in transport, resulting in coastal advancement (Bosboom & Stive, 2023).

In this study, the XBeach 2DH model was employed to estimate the LST rate along the coastline of GB. Buttò et al. (*submitted*) have proposed an XBeach 2DH model calibrated using field measurements of the LST rate. The resulting model is the most accurate methodology for predicting the LST rate compared to commonly used bulk formulas. The strengths of this model consist of its ability to account for the specific characteristics of the study area that influence the LST rate, such as wave parameters, grain size, seabed/emerged morphology, and the presence of marine vegetation (Buttò et al., *submitted*). We realized XBeach 2DH models using the calibrations proposed by Buttò et al. (*submitted*; tab. S1) to calculate the LST rate for average wave conditions of the study areas. We used the Surfbeat module in the 1.24.6057 Halloween XBeach release.

Regarding the wave boundary conditions, we chose the JONSWAP spectrum and performed a 12h simulation. To obtain the optimal performance of XBeach 2DH models, the wave data closest to the coastline is used, and the model grid is extended seaward to the point corresponding to the wave data location (Buttò et al., *submitted*). The Copernicus database provides the input wave parameters (see section 3.1). To generate the model grid and merge bathymetric and topographic datasets, we used the Deltares Open Earth Toolbox in MATLAB (*Deltares OpenEarth Matlab Toolbox*, n.d.). We set a grid with variable-size cells in x direction (tab. S2). The grid consists of cells with a maximum size of 10 in sectors with water depths greater than the depth of closure. For water depths minor than the depth of closure, the cell size decreases landward from the maximum value to the minimum of 0.5 m (see tab S2 for the other parameter sets of computational domains). Local wind and tidal set-up were not considered in the model set-up. The sediment transport rate was calculated using the Van Rijn equations (Van Rijn, 1993). The initial water level (z0) was set to zero, the morphological acceleration factor (morfac) was set to 1, and the simulation time was adapted to the morfac (morfacopt=1). The parameters having the most significant influence on LST were set using values proposed by Buttò et al. (*submitted*; tab. S1).

To evaluate the vulnerability of a coastline to LST, we consider that higher transport levels correspond to increased vulnerability. The vulnerability classes related to the LST rate are defined in Table 4 concerning the results obtained by the XBeach 2DH model for mean wave condition.

3.2.4 Wave Height (WH)

Waves are a key factor in forming longitudinal and transverse coastal currents, significantly influencing erosional processes. Larger wave heights break with higher energy on beaches, mobilizing greater volumes of sediment and inducing significant morphodynamic changes (Abuodha & Woodroffe, 2010; Mohamed, 2020).

The maximum H_o ($H_{o,max}$) was used to assess the vulnerability related to the WH sub-index, following the vulnerability ranking proposed by Gornitz (Gornitz et al., 1991), as shown in Table 5.

3.3 Coastal Vulnerability Index

The CVI is calculated to identify areas most vulnerable to erosion. The most used method to calculate the CVI is the square root of the product mean of the scores assigned to each sub-indexes (Addo, 2013; Gornitz et al., 1991; B. E. A. Pendleton et al., 2005; E. Pendleton et al., 2004; Rani et al., 2018; Theocharidis et al., 2024; Thieler & Hammar-Klose, 1999). Following this method, in this study, we calculate the CVI by using the equation (2):

$$CVI = \sqrt{[\frac{MC*SD*LST*WH}{4}]} \quad (2)$$

The CVI ranking is based on vulnerability classes obtained by dividing into 33 percentile ranges the total ranges of CVI values (tab. 6). The results were used to obtain a vulnerability map.

4. Results

We followed the steps of the procedure shown in Table 1 to apply the proposed method. After collecting data (first step), we divided the study area into four sections (fig. 3; second step), and we calculated the sub-indexes (third step) and CVI (fourth step).

The slope of the seabed exhibited slight variations, with values between 0.9% in Section 4 (S4) and 1.5% in Section 1 (S1, tab. 7). The width of the emerged beach ranged from 35.0 m in S1 to 47.9 m in Section 2 (S2) while headlands were present in both part of the beach, measuring 3075.3 m and 2367.7 m beside S1 and 4, respectively (tab. 7). All sections contained marine vegetation, while dune systems were absent across all sections (tab. 7).

The seabed slope indicated a very low vulnerability across all sections (rank 1; fig. 4a). Beach width vulnerability ranged from moderate in S2, Section 3 (S3) and S4 (rank 3) to high in S1 (rank 4; fig. 4a). Concerning to presence of headlands and marine vegetation, results showed the highest and the lowest vulnerability values for the whole area, respectively (rank 5 and 1; fig. 4a). Due to the absence of dune systems, all sections showed a very high vulnerability rank (rank 5; fig. 4a) for this parameter. The calculated values of the MC sub-index show a vulnerability rank of 3 (moderate) for all sections (fig. 4b).

Concerning the SD sub-index, we calculate the v_o of the coastline over different time intervals (tab. 8). S1 experienced v_o in MR of -4.3 m/y (the minus sign indicates a coastline retreat), while ST, MT, and LT experienced v_o of about -1m. S2 showed the highest v_o of -7.5 m/y for the MR term and -1.5, -1 and -0.6 m/y for ST, MT and LT, respectively. In contrast, S3 showed no significant v_o across all periods. S4 displayed shoreline retreat in MR (v_o -4.3 m/y) and MT (v_o -2.2 m/y), with almost no variation in the ST and LT (v_o -0.1 m/y).

The vulnerability rankings for SD shows that S1, S2, and S4 had the highest vulnerability for the MR period (rank 5), while S3 was classified as moderately vulnerable (rank 3; fig. 5a). The ST period showed high vulnerability in S1 and S2 (rank 4), whereas S3 and S4 had moderate vulnerability (rank 3; fig. 5a). MT vulnerability ranked from moderate in S1 and S3 (rank 3), to high in S2 (rank 4) and very high in S4 (rank 5; fig. 5a). LT vulnerability remained consistent across all sections (rank 3; fig. 5a). The SD sub-index vulnerability values were 4 in S1, S2, and S4, while S3 showed moderate vulnerability (rank 3; fig. 5b).

An analysis of wave climate data was conducted to identify the most frequent wave conditions over 30 years. In the first phase of the analysis, the data were categorised into wave height intervals of 0.5 m and direction intervals of 10°. Results showed that the most frequent waves (18.7%) came from a D_{ir} of 320°N, and the H_o occurring most frequently (5.9%) was between 0.5 and 1 m (fig. 6). A second phase of analysis focused on waves from 315-325°N with H_o between 0.5 and 1 m to find the most frequent value of H_o and the mean T_p value. The obtained wave parameters were H_o of 0.77 m, T_p of 5.94 s, and D_{ir} 320°N.

We used mean wave parameters to calculate the LST rate along the shoreline for studied sections (S1 to S4) using XBeach 2DH model (fig. 7a). S1 recorded a mean LST rate of 0.07 kg/s. S2 displayed a mean LST rate of -0.06 kg/s; the minus sign indicates an opposite sediment transport direction in this section. S3 showed a minimal LST rate, with values close to 0 kg/s (0.0001 kg/s). S4 recorded the highest LST rate of 0.34 kg/s.

Results of vulnerability related to the LST sub-index (fig. 7b) show that S4 exhibited moderate vulnerability (rank 3), while S1, S2 and S3 marked very low vulnerability levels (rank 1).

The dataset of wave climate was analyzed to determine the $H_{o,max}$ recorded. The $H_{o,max}$ was 7.02 m. According to Gornitz's vulnerability classification (1991; tab.5) for $H_{o,max}$, the vulnerability of the entire area to the WH sub-index is classified as very high, corresponding to a rank 5 (fig. 8).

The sub-index values were combined to calculate the CVI for the studied sections. The resulting CVI values were 3.9, 3.9, 3.4, and 6.7 for S1, S2, S3, and S4, respectively. The vulnerability levels associated with these values indicate low vulnerability for S1, S2 and S3, while S4 exhibits moderate vulnerability (fig. 9).

5. Discussions

Applying the proposed CVI allows for delineating the most vulnerable areas to erosion along the Għadira Bay coastline. The CVI map (fig. 9) highlights that S1, S2 and S3 are low vulnerable to erosion, while S4 show moderate vulnerability.

S4 has moderate to high vulnerability for most indices, with a final CVI of 6.7. The key factor that affects the result is the LST value, which is significantly higher than other sections. The values of other sub-indexes are very similar in all sections. The presence of large promontories and the absence of dune systems determined a very high vulnerability (rank 5) of the entire area, while the marine vegetation and the slope lowered the overall vulnerability (fig. 4a-b). Regarding the SD sub-index, MR and ST periods mainly contribute to determining this index's high vulnerability value in sections S1, S2 and S4 (figure 5a-b). Section S3 instead records no variation in the coastline in all the periods considered, probably linked to the rocky seabed in this section (fig. 5a-b). Finally, the wave climate analysis showed that the Għadira Bay area was affected by waves with H_o up to 7m. This condition determined a very high vulnerability ranking relative to the WH sub-index for all sections (fig. 8).

From a methodological point of view, the CVI presented in this study tried to overcome the limitations of previous approaches (Arun Kumar & Kunte, 2012; Coelho et al., 2006; Ietto et al., 2018) that neglected parameters that directly influence the system's ability to balance sediment loss and input (e.g., the presence of headlands and marine vegetation). Furthermore, physical processes (e.g., waves and currents) that drive the sediment dynamics of the submerged beach sector need to be included. For these reasons, the present study used new sub-indexes (MC and LST) in addition to those used by previous researchers (SD and WH), which allows for assessing the vulnerability of the beach to erosion more precisely.

Previous studies' most relevant vulnerability sub-indexes are mean significant wave height, geomorphology and geology. Different researchers have used these sub-indexes as an indirect proxy of LST. The mean significant wave height sub-index was considered an indicator of the wave energy that drives the LST (Rani et al., 2018; Yin et al., 2012). Geomorphology and geology sub-indexes were used as expressions of the relative degree of erosion of different landforms (e.g. rocky cliffs, beaches or flood plains) and rock types (e.g. plutonic, metamorphics and sedimentary rocks or unconsolidated sediments) (Özyurt & Ergin, 2010; Rani et al., 2018; Rocha et al., 2020). In this work, the indicators that qualitatively and indirectly estimate the LST are not considered (e.g., mean significant wave height, geomorphology, and geology) because we decided to introduce the LST sub-index. We calculated the LST rate related to mean significant wave conditions using XBeach 2DH numerical model, which is the most accurate method to estimate the LST rate compared to field data (Buttò et al. *submitted*). In this way, we could identify LST rate gradients along the coastline and estimate LST more accurately than previous methodologies.

In this study, we proposed a reformulated MC sub-index. Previous studies have included MC estimation for vulnerability assessment. However, these studies aim to assess the vulnerability to flooding caused by rising sea levels, tsunamis, and storm surges (Satta et al., 2016; Torresan et al., 2012). The most commonly used parameters for this purpose were topographic elevation and emerged beach slope (López Royo et al., 2016; Rani et al., 2018; Szlafsztein & Sterr, 2007; Torresan et al., 2012). Since the study of flood vulnerability is not the subject of this work, we chose not to consider the related parameters and to reformulate the MC sub-index to include variables (qualitative and quantitative) that constitute a natural coastal defence system from erosion.

For the MC sub-index estimation, three parameters concerning the characteristics of the emerged coastal part and two parameters concerning the submerged part were considered: length of the headlands, width of the beach, presence of dune systems, seabed slope and presence of marine vegetation. The presence of headlands can interfere with sediment transport, leading to local changes in the coastline. The vulnerability of the beach to erosion increases with the increase of headland length. Natural dune systems reduce the vulnerability of sandy beaches to storm surges and coastal erosion compared to areas without dunes (McLaughlin et al., 2010). Therefore, vulnerability increases when dunes are absent. We also considered the beach width as a variable of the MC sub-index because narrower beaches are more vulnerable than wider ones.

Regarding the measure of the slope of the submerged beach, we chose to include it in the definition of the MC sub-index because the slope affects erosion. A lower beach slope induces greater wave energy dissipation offshore, reducing the wave energy entering the shallower waters (Dionísio António et al., 2023). The greater the slope, the greater the sediment transport in the swash zone under the same wave conditions (Dionísio António et al., 2023). Finally, the presence of marine vegetation is included. Most previous studies have considered only the presence of vegetation in emerged area (Arun Kumar & Kunte, 2012; Myers et al., 2019; Rizzo et al., 2020; Satta et al., 2016; Yin et al., 2012) or intermediate environments such as coastal salt marshes (Szlafsztein & Sterr, 2007). Marine vegetation constitutes a natural defence system against sediment erosion, reducing shear stress at the sediment-water interface (Le Hir et al., 2007; Widdows & Brinsley, 2002). Consequently, vulnerability increases if the seabed lacks vegetation or has poor cover.

Furthermore,–we have included the SD and WH sub-indexes following previous studies (Acevedo, 2019; Coelho et al., 2006; Gornitz et al., 1991; Sahoo & Bhaskaran, 2018; Shaw et al., 1998; Theocharidis et al., 2024). SD sub-index is used to represent the coastal dynamics accumulated over time in order to provide a reference for the variability of coastline position on different time scales. Furthermore, we included the WH sub-index to capture the potential impact of extreme wave events on coastal erosion. While the LST sub-index accounts for the mean wave climate, the WH sub-index assesses the vulnerability of beaches during storm events, which are known to intensify erosive processes and cause significant shoreline retreat (Do & Yoo, 2020; Karunarathna et al., 2014).

Future studies could extend the proposed CVI by a) testing the proposed CVI in coastal areas with different characteristics (e.g. open systems and/or gravel beaches), b) including projections of future sea level change and c) other variables relevant to the sediment budget of beaches, such as river sediment input.

6. Conclusions

This study proposes a CVI to erosion of beaches by combining four sub-indexes (MC, SD, LST and WH), several datasets and techniques, including XBeach 2DH numerical model and GISs. The proposed index has been tested in Għadira Bay, revealing that this coastline is affected by low vulnerability to erosion in the north and central sectors and moderate in the southern.

The CVI developed in this study significantly improves previous methodologies by offering a more precise representation of beach vulnerability to erosion by considering two parameters that directly affect the balance between sediment loss and input: headland's length and marine vegetation. Moreover, the methodology includes the LST sub-index, which was quantitatively assessed using the XBeach 2DH numerical model. This method differs from previous studies that indirectly evaluate the LST through factors of control like the mean significant wave height, geomorphology, and geology. Thus, using the LST sub-index allowed us to achieve a more detailed and reliable vulnerability assessment.

This study provided a new CVI as a helpful tool to assess the vulnerability to erosion in coastal areas such as Għadira Bay. The approach offers valuable support to government organizations in assessing coastal risk conditions. This methodology can be used to plan protection interventions to safeguard coastal communities, infrastructures and cultural heritage present in coastal areas.

References

Abuodha, P. A. O., & Woodroffe, C. D. (2010). Assessing vulnerability to sea-level rise using a coastal sensitivity index: A case study from southeast Australia. *Journal of Coastal Conservation*, *14*(3), 189–205. https://doi.org/10.1007/s11852-010-0097-0

Acevedo, D. (2019). *A Review of Coastal Vulnerability Assessments: Definitions, Components, and Variables Environmental Laboratory A Review of Coastal Vulnerability Assessments: Definitions, Component... Restoring and Maintaining Salt Marshes in the Face of Sea Level Rise Vi*. www.erdc.usace.army.mil.

Addo, K. A. (2013). Assessing Coastal Vulnerability Index to Climate Change: the Case of Accra – Ghana. *Journal of Coastal Research*, *165*, 1892–1897. https://doi.org/10.2112/si65-320.1

Arun Kumar, A., & Kunte, P. D. (2012). Coastal vulnerability assessment for Chennai, east coast of India using geospatial techniques. *Natural Hazards*, *64*(1), 853–872. https://doi.org/10.1007/s11069-012-0276-4

Balica, S. F., Wright, N. G., & van der Meulen, F. (2012). A flood vulnerability index for coastal cities and its use in assessing climate change impacts. In *Natural Hazards* (Vol. 64, Issue 1). https://doi.org/10.1007/s11069-012-0234-1

Boak, E. H., & Turner, I. L. (2005). Shoreline definition and detection: a review. *Journal of Coastal Research*, *21*(4), 688–703.

Borg, J. A., Attrill, M. J., Rowden, A. A., Schembri, P. J., & Jones, M. B. (2005). Architectural characteristics of two bed types of the seagrass Posidonia oceanica over different spatial scales. *Estuarine, Coastal and Shelf Science*, *62*(4), 667–678. https://doi.org/10.1016/j.ecss.2004.10.003

Bosboom, J., & Stive, M. J. F. (2023). Coastal dynamics. In *Delft University of Ttchnology, Delft, The Netherlands. Publisher*. TU Delft Open. https://doi.org/10.5074/t.2021.001

Bourne, A., Holness, S., Holden, P., Scorgie, S., Donatti, C. I., & Midgley, G. (2016). A socio-ecological approach for identifying and contextualising spatial ecosystem-based adaptation priorities at the sub-national level. *PLoS ONE*, *11*(5), 1–21. https://doi.org/10.1371/journal.pone.0155235

Buttò, S., Faraci, C. L., Corradino, M., Iuppa, C., Colica, E & Pepe, F. (*submitted*).

Evaluating Longshore Sediment Transport: a comparison between empirical formulas and XBeach 2DH numerical model. *Marine Geology*

Coelho, C., Silva, R., Veloso-Gomes, F., & Pinto, F. T. (2006). A vulnerability analysis approach for the Portuguese West Coast. *WIT Transactions on Ecology and the Environment*, *91*, 251–262. https://doi.org/10.2495/RISK060241

Deltares OpenEarth Matlab Toolbox (p. https://svn.oss.deltares.nl/repos/openearthtools/t). (n.d.). https://svn.oss.deltares.nl/repos/openearthtools/trunk/matlab/

Dionísio António, S., van der Werf, J., Horstman, E., Cáceres, I., Alsina, J., van der Zanden, J., & Hulscher, S. (2023). Influence of Beach Slope on Morphological Changes and Sediment Transport under Irregular Waves. *Journal of Marine Science and Engineering*, *11*(12). https://doi.org/10.3390/jmse11122244

Do, K., & Yoo, J. (2020). Morphological response to storms in an embayed beach having limited sediment thickness. *Estuarine, Coastal and Shelf Science*, *234*(February), 106636. https://doi.org/10.1016/j.ecss.2020.106636

Doukakis, E. (2005). Identifying Coastal Vulnerability Due to Climate Changes. *Journal of Marine Environmental Engineering*, *8*(2).

Drago, A. F., Azzopardi, J., Gauci, A., Bruschi, A., R, T., & Bruschi, A. (2013). Assessing the offshore wave energy potential for the Maltese islands. *ISE Annual Conference*, *March*.

Galdies, C. (2011). *The Climate of Malta: statistics, trends and analysis 1951-2010* (Issue August 2011).

Gornitz, V. (1990). Vulnerability of the East Coast, USA to future sea level rise. *Journal of Coastal Research*, 201–237.

Gornitz, V., White, T. W., Cushman, R. M., Rivki, M., Bachtiar, A. M., Informatika, T., Teknik, F., & Indonesia, U. K. (1991). *Vulnerability of the US to future sea level rise* (Issue 112). Oak Ridge National Lab., TN (USA).

Hallermeier, R. (1981). A profile zonation for seasonal sand beaches from wave climate. *Coastal Eng.*, *4*, 253–277.

Ietto, F., Cantasano, N., & Pellicone, G. (2018). A New Coastal Erosion Risk Assessment Indicator: Application to the Calabria Tyrrhenian Littoral (Southern Italy).

Environmental Processes, *5*(2), 201–223. https://doi.org/10.1007/S40710-018-0295-6/FIGURES/7

Karunarathna, H., Pender, D., Ranasinghe, R., Short, A. D., & Reeve, D. E. (2014). The effects of storm clustering on beach profile variability. *Marine Geology*, *348*(November 2015), 103–112. https://doi.org/10.1016/j.margeo.2013.12.007

Kleini, R. T., Smit, M., & Goosen, H. (2016). *Resilience and Vulnerability: Coastal Dynamics or Dutch Dikes? 164*(3), 259–268.

Korres, G., Oikonomou, C., Denaxa, D., & Sotiropoulou, M. (2023). *Mediterranean Sea Waves Analysis and Forecast (Copernicus Marine Service MED-Waves, MEDWAM4 system) (Version 1) [Data set]*. Copernicus Monitoring Environment Marine Service (CMEMS). https://doi.org/https://doi.org/10.25423/CMCC/MEDSEA_ANALYSISFORECAST_WAV_006_017_MEDWAM4

Le Hir, P., Monbet, Y., & Orvain, F. (2007). Sediment erodability in sediment transport modelling: Can we account for biota effects? *Continental Shelf Research*, *27*(8), 1116–1142. https://doi.org/10.1016/j.csr.2005.11.016

López Royo, M., Ranasinghe, R., & Jiménez, J. A. (2016). A rapid, low-cost approach to coastal vulnerability assessment at a national level. *Journal of Coastal Research*, *32*(4), 932–945.

Masson-Delmotte, V., Zhai, P., Pörtner, H.-O., Roberts, D., Skea, J., Shukla, P. R., Pirani, A., Moufouma-Okia, W., Péan, C., & Pidcock, R. (2019). Global warming of 1.5 C. *An IPCC Special Report on the Impacts of Global Warming Of*, *1*, 93–174.

McLaughlin, S., Andrew, J., & Cooper, G. (2010). A multi-scale coastal vulnerability index: A tool for coastal managers? *Environmental Hazards*, *9*(3), 233–248. https://doi.org/10.3763/ehaz.2010.0052

McLaughlin, S., McKenna, J., & Cooper, J. A. G. (2002). Socio-economic data in coastal vulnerability indices: constraints and opportunities. *Journal of Coastal Research*, *36*, 487–497.

Mcleod, E., Poulter, B., Hinkel, J., Reyes, E., & Salm, R. (2010). Sea-level rise impact models and environmental conservation: A review of models and their applications. *Ocean and Coastal Management*, *53*(9), 507–517.

https://doi.org/10.1016/j.ocecoaman.2010.06.009

Mohamed, S. (2020). Coastal vulnerability assessment using GIS-Based multicriteria analysis of Alexandria-northwestern Nile Delta, Egypt. *Journal of African Earth Sciences*, *163*, 103751. https://doi.org/10.1016/j.jafrearsci.2020.103751

Myers, M. R., Barnard, P. L., Beighley, E., Cayan, D. R., Dugan, J. E., Feng, D., Hubbard, D. M., Iacobellis, S. F., Melack, J. M., & Page, H. M. (2019). A multidisciplinary coastal vulnerability assessment for local government focused on ecosystems, Santa Barbara area, California. *Ocean and Coastal Management*, *182*(September), 104921. https://doi.org/10.1016/j.ocecoaman.2019.104921

Oliveira, F. S. B. F., Fortunato, A. B., & Freire, P. M. S. (2021). *Analysis of S. João da Caparica beach vulnerability to a maritime storm event*. *May*.

Özyurt, G., & Ergin, A. (2010). Improving coastal vulnerability assessments to sea-level rise: A new indicator-based methodology for decision makers. *Journal of Coastal Research*, *26*(2), 265–273. https://doi.org/10.2112/08-1055.1

Pendleton, B. E. A., Thieler, E. R., Williams, S. J., Norton, G. A., Survey, U. S. G., & Beavers, R. (2005). *Coastal vulnerability assessment of golden gate national recreation area to sea-level rise*.

Pendleton, E., Thieler, E., & Williams, S. (2004). Coastal vulnerability assessment of Cumberland Island National Seashore (CUIS) To sea-level rise. *US Geological Survey Open-File Report 2004-1196*, 1–23.

Ramieri, E., Hartley, A., Office, M., Barbanti, A., National, I., & Santos, F. D. (2011). *Methods for assessing coastal vulnerability to climate change ETC CCA Technical Paper 1 / 2011*. *January*. https://doi.org/10.13140/RG.2.1.1906.9840

Rani, M., Rehman, S., Sajjad, H., Chaudhary, B. S., Sharma, J., Bhardwaj, S., & Kumar, P. (2018). Assessing coastal landscape vulnerability using geospatial techniques along Vizianagaram–Srikakulam coast of Andhra Pradesh, India. *Natural Hazards*, *94*(2), 711–725. https://doi.org/10.1007/s11069-018-3414-9

Rizzo, A., Vandelli, V., Buhagiar, G., Micallef, A. S., & Soldati, M. (2020). Coastal vulnerability assessment along the north-eastern sector of Gozo Island (Malta, Mediterranean Sea). *Water (Switzerland)*, *12*(5). https://doi.org/10.3390/w12051405

Rocha, C., Antunes, C., & Catita, C. (2020). Coastal vulnerability assessment due to sea level rise: The case study of the Atlantic coast of Mainland Portugal. *Water (Switzerland)*, *12*(2). https://doi.org/10.3390/w12020360

Sahoo, B., & Bhaskaran, P. K. (2018). Multi-hazard risk assessment of coastal vulnerability from tropical cyclones – A GIS based approach for the Odisha coast. *Journal of Environmental Management*, *206*, 1166–1178. https://doi.org/10.1016/j.jenvman.2017.10.075

Satta, A., Snoussi, M., Puddu, M., Flayou, L., & Hout, R. (2016). An index-based method to assess risks of climate-related hazards in coastal zones: The case of Tetouan. *Estuarine, Coastal and Shelf Science*, *175*, 93–105. https://doi.org/10.1016/j.ecss.2016.03.021

Serafim, M. B., Siegle, E., Corsi, A. C., & Bonetti, J. (2019). Coastal vulnerability to wave impacts using a multi-criteria index: Santa Catarina (Brazil). *Journal of Environmental Management*, *230*(September 2018), 21–32. https://doi.org/10.1016/j.jenvman.2018.09.052

Shaw, J., Taylor, R. B., Forbes, D. L., Ruz, M. H., & Solomon, S. (1998). *Sensitivity of the coasts of Canada to sea-level rise*. Geological Survey of Canada Ottawa.

Siegle, E., & Asp, N. E. (2007). WAVE REFRACTION AND LONGSHORE TRANSPORT PATTERNS ALONG THE SOUTHERN SANTA CATARINA COAST. *Brazilian Journal of Oceanography*, *55*(2), 109 – 120. https://doi.org/10.1590/s1679-87592007000200004

Szlafsztein, C., & Sterr, H. (2007). A GIS-based vulnerability assessment of coastal natural hazards, state of Pará, Brazil. *Journal of Coastal Conservation*, *11*(1), 53–66. https://doi.org/10.1007/s11852-007-0003-6

Theocharidis, C., Doukanari, M., Kalogirou, E., Christofi, D., Mettas, C., Kontoes, C., Hadjimitsis, D., Argyriou, A. V, & Eliades, M. (2024). Coastal Vulnerability Index (CVI) Assessment: Evaluating Risks Associated with Human-Made Activities along the Limassol Coastline, Cyprus. *Remote Sensing*, *16*(19), 3688. https://doi.org/10.3390/rs16193688

Thieler, E. R., & Hammar-Klose, E. S. (1999). *National assessment of coastal vulnerability to sea-level rise: preliminary results for the US Atlantic coast*. US Geological survey.

Torresan, S., Critto, A., Rizzi, J., & Marcomini, A. (2012). Assessment of coastal vulnerability to climate change hazards at the regional scale: The case study of the North Adriatic Sea. *Natural Hazards and Earth System Science*, *12*(7), 2347–2368. https://doi.org/10.5194/nhess-12-2347-2012

Van Rijn, L. C. (1993). *Principles of sediment transport in rivers, estuaries and coastal seas*. International Institute for Infrastructural, Hydraulic, and Environmental Engineering, Delft, The Netherlands.

Wamsler, C., Luederitz, C., & Brink, E. (2014). Local levers for change: Mainstreaming ecosystem-based adaptation into municipal planning to foster sustainability transitions. *Global Environmental Change*, *29*, 189–201. https://doi.org/10.1016/j.gloenvcha.2014.09.008

Widdows, J., & Brinsley, M. (2002). Impact of biotic and abiotic processes on sediment dynamics and the consequences to the structure and functioning of the intertidal zone. *Journal of Sea Research*, *48*(2), 143–156. https://doi.org/10.1016/S1385-1101(02)00148-X

Yin, J., Yin, Z., Wang, J., & Xu, S. (2012). National assessment of coastal vulnerability to sea-level rise for the Chinese coast. *Journal of Coastal Conservation*, *16*(1), 123–133. https://doi.org/10.1007/s11852-012-0180-9

Captions

Table 1. *Flowchart of the Coastal Vulnerability Index calculation method.*

Table 2. *Vulnerability classes for the evaluation of the Morphological Characteristics (MC) sub-index.*

Table 3. *Vulnerability classes for evaluating the Shoreline Displacement (SD) sub-index (after Gornitz et al., 1991).*

Table 4. *Vulnerability classes for assessing the Longshore Sediment Transport (LST) sub-index.*

Table 5. *Vulnerability classes for evaluating the Wave Height (WH) sub-index after Gornitz (1991).*

Table 6. *The CVI ranking.*

Table 7. *Measured values of parameters related to MC sub-indexes calculated in each section.*

Table 8. *Measured values of parameters related to SD sub-indexes calculation. The minus sign indicates a retreat of the coastline.*

Table S1. *Calibrated parameters and used values to calibrate XBeach 2DH model of Għadira Bay (Buttò et al., submitted).*

Table S2. *Main XBeach parameter set.*

Figure 1. *Geographic location of Għadira Bay. In a) the location of the Maltese archipelago in the Mediterranean area. In b) Għadira Bay's location in Malta Island's northeastern sector.*

Figure 2. *Coastline positions of different years, represented by dashed lines of different colours.*

Figure 3. *Measurement sections into which Għadira Bay has been divided. The red line shows the landward measurement boundary, represented by the sea wall. The black line represents the seaward measurement boundary and the depth of closure.*

Figure 4. *Vulnerability map related to MC sub-index. In a) vulnerability ranking to each measured parameter. In b) vulnerability ranking to MC sub-index.*

Figure 5. *Vulnerability map related to SD sub-index. In a) vulnerability ranking to each measured parameter. In b) vulnerability ranking to SD sub-index.*

Figure 6. Rose diagram illustrates the distribution of wave heights (H_0) across different directions in percentage for Għadira Bay.

Figure 7. *a) LST rate calculated using XBeach 2DH model and b) vulnerability ranking of LST sub-index.*

Figure 8. *Vulnerability ranking of WH sub-index.*

Figure 9. *The CVI to erosion of Għadira Bay.*

Tables

Table 1.

Step 1	**Collection of variables needed to calculate the sub-indexes**			
	DEMs, orthophoto, bathymetric maps and marine vegetation maps.	Orthophotos, satellite images and aerial photos.	Grain size data, wave data (e.g., significant wave height, period and direction).	Wave data (e.g., significant wave height, period and direction).
Step 2	**Subdivision of the beach in sectors**			
Step 3	**Calculation of sub-indexes**			
	Morphological Characteristics (MC)	Shoreline Displacement (SD)	Longshore Sediment Transport (LST)	Wave Height (WH)
Step 4	**Coastal Vulnerability Index estimation**			

Table 2.

Sub-index		Vulnerability Rank				
		Very low	Low	Moderate	High	Very High
		1	2	3	4	5
Morphological Characteristics	Slope seabed (%)	<2	2-6	6-10	10-20	≥20
	Width emerged beach (m)	≥ 80	80-60	60-40	40-20	<20
	Headland's length (m)	≥0 and < 187.5	≥187.5 and <375	≥375 and <562.5	≥562.5 and <750	≥750
	Marine vegetation	Presence	-	-	-	Absence
	Dune systems	Presence	-	-	-	Absence

Table 3.

Sub-index		Vulnerability Rank					Weight
		Very low	Low	Moderate	High	Very High	
		1	2	3	4	5	
Shoreline displacement (m/y)	MR	> 2	>1 and ≤ 2	>-1 and ≤ +1	>-2 and ≤ -1	≥ -2	0.4
	ST	> 2	>1 and ≤ 2	>-1 and ≤ +1	>-2 and ≤ -1	≥ -2	0.3
	MT	> 2	>1 and ≤ 2	>-1 and ≤ +1	>-2 and ≤ -1	≥ -2	0.2
	LT	> 2	>1 and ≤ 2	>-1 and ≤ +1	>-2 and ≤ -1	≥ -2	0.1

Table 4.

Sub-index	Vulnerability Rank				
	Very low	Low	Moderate	High	Very High
	1	2	3	4	5
Longshore Sediment Transport (kg/s)	≥0 and <0.125	≥0.125 and <0.25	≥0.25 and < 0.375	≥0.375 and <0.5	≥0.5

Table 5.

Sub-index	Vulnerability Rank				
	Very low	Low	Moderate	High	Very High
	1	2	3	4	5
Wave Height (m)	≥0 and <2.9	≥3 and <4.9	≥5 and <5.9	≥6 and <6.9	≥7

Table 6.

CVI rank		
Low	Moderate	High
≥ 0 and < 3.9	≥ 4 and < 7.9	≥ 8

Table 7.

Sub-index		Measured value			
		Section 1	Section 2	Section 3	Section 4
Morphological Characteristics	Slope seabed (%)	1.5	1.3	1.1	0.9
	Width emerged beach (m)	35.0	47.9	41.7	41.3
	Headland's length (m)	3075.3	-	-	2367.7
	Marine vegetation	present	present	present	present
	Dune systems	absent	absent	absent	absent

Table 8.

Sub-index		Measured value			
		Section 1	Section 2	Section 3	Section 4
Shoreline Displacement	MR (m/y)	-4.3	-7.5	0.0	-4.3
	ST (m/y)	-1.2	-1.5	0.0	-0.1
	MT (m/y)	-0.7	-1.0	0.0	-2.2
	LT (m/y)	-1.0	-0.6	0.0	-0.1

Table S1.

Parameter	Description	Default value	Used value
facua	Calibration factor time averaged flows due to wave skewness and asymmetry	0.175	0.35
alfaD50	Calibration coefficient for grain size term	0.4	0.25
bdslpeffmag	Modify the magnitude of the sediment transport based on the bed slope	roelvink_total	soulsby_bed
facsl	Factor bedslope effect	1.6	1.6
bdslpeffini	Modify the critical shields parameter based on the bed slope	none	total
reposeangle	Angle of internal friction	30	30
form	Equilibrium sediment concentration formulation	vanthiel_vanrijn	Vanrijn1993
lws	Switch to enable long wave stirring	1	0
turb	Switch to include short wave turbulence	wave_averaged	none
wetslp	Critical avalanching slope under water	0.15	0.15
morfac	Morphological acceleration factor	1	1
morfacopt	Switch to adjusting output times for morfac	1	1

Table S2.

Parameter	Description	Value
nx	Number of computational cell corners in cross-shore direction	651
ny	Number of computational cell corners in longshore direction	119
dx_{max}/dx_{min}	Dimensions of cell in cross-shore direction	10 - 0.5m
dy	Dimensions of cell in longshore direction	15m
thetamin	Lower directional limit	315
thetamax	Higher directional limit	325
dtheta	Directional resolution	5

Figures

Figure 1.

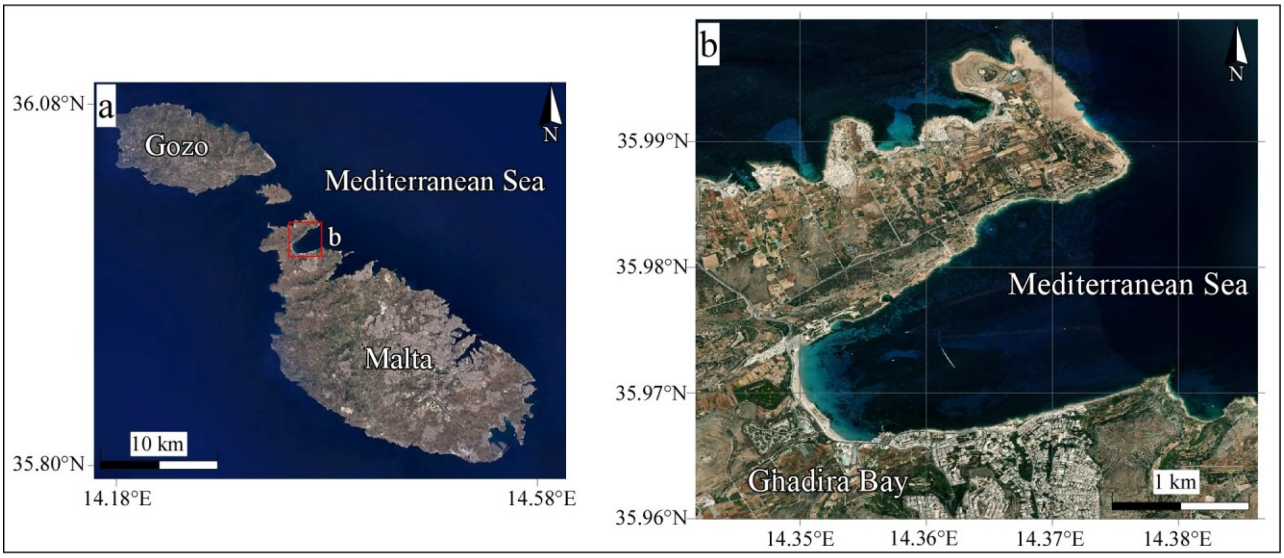

Figure 2.

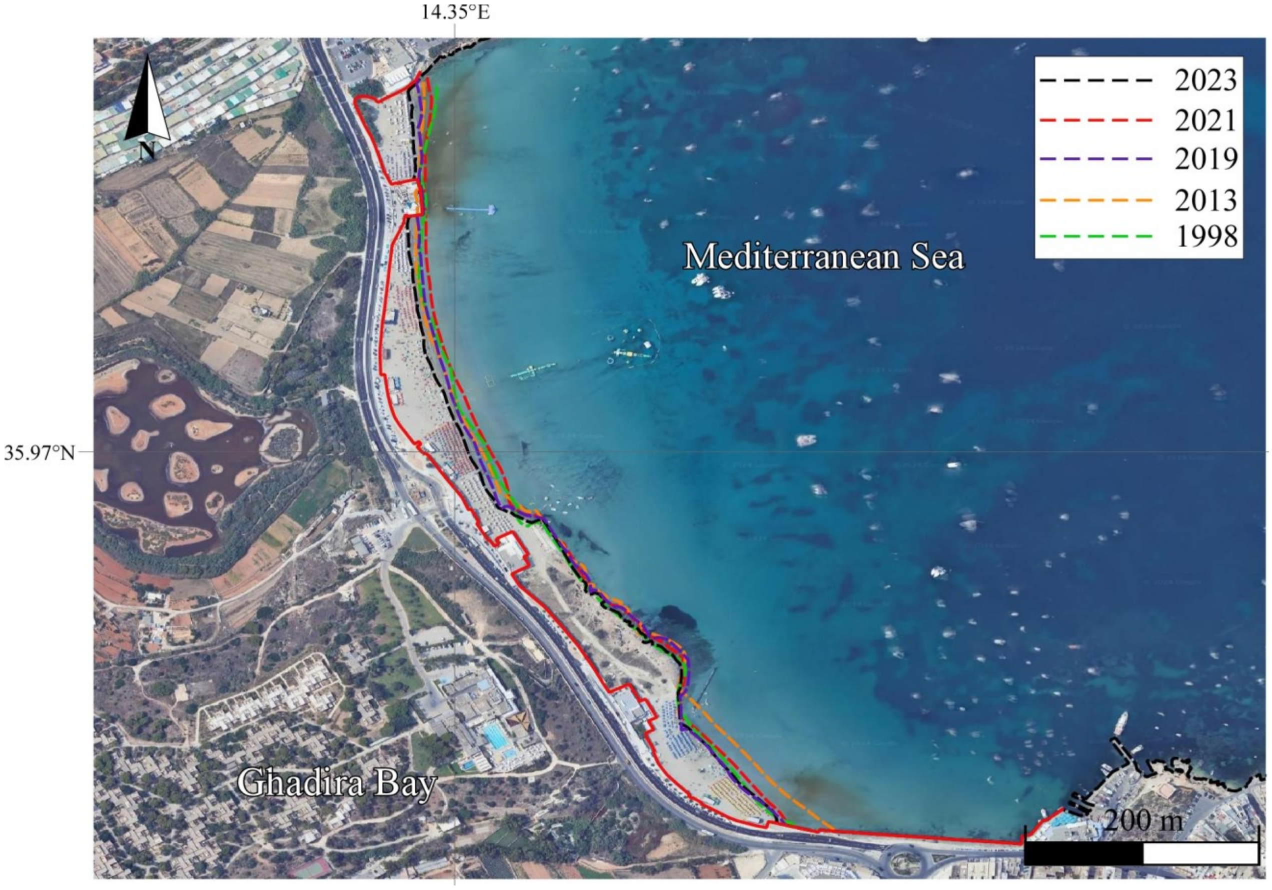
14.35°E
35.97°N
N
2023
2021
2019
2013
1998
Mediterranean Sea
Ghadira Bay
200 m

Figure 3.

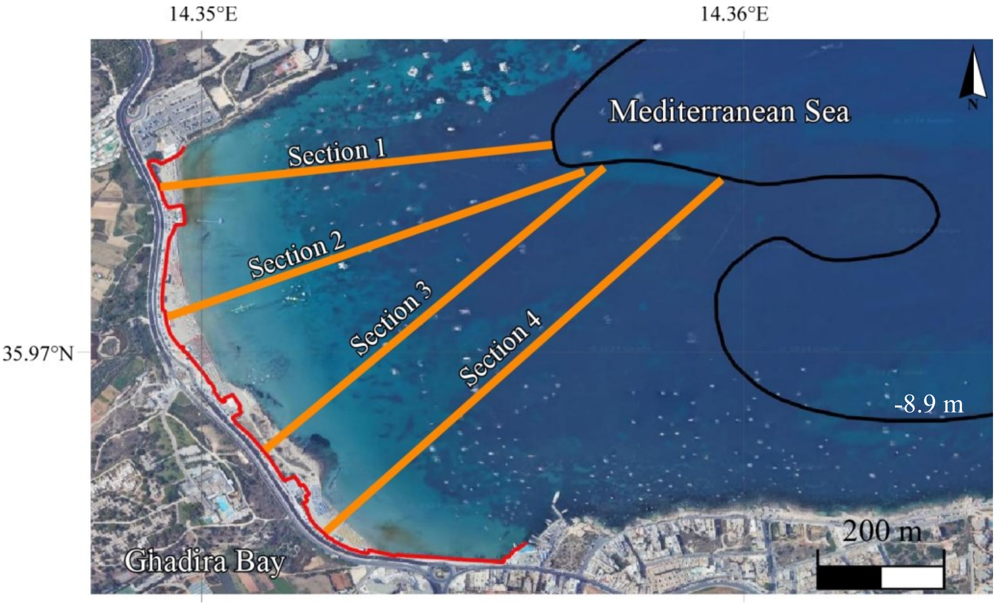
14.35°E
14.36°E
35.97°N
Mediterranean Sea
N
Section 1
Section 2
Section 3
Section 4
-8.9 m
200 m
Ghadira Bay

Figure 4.

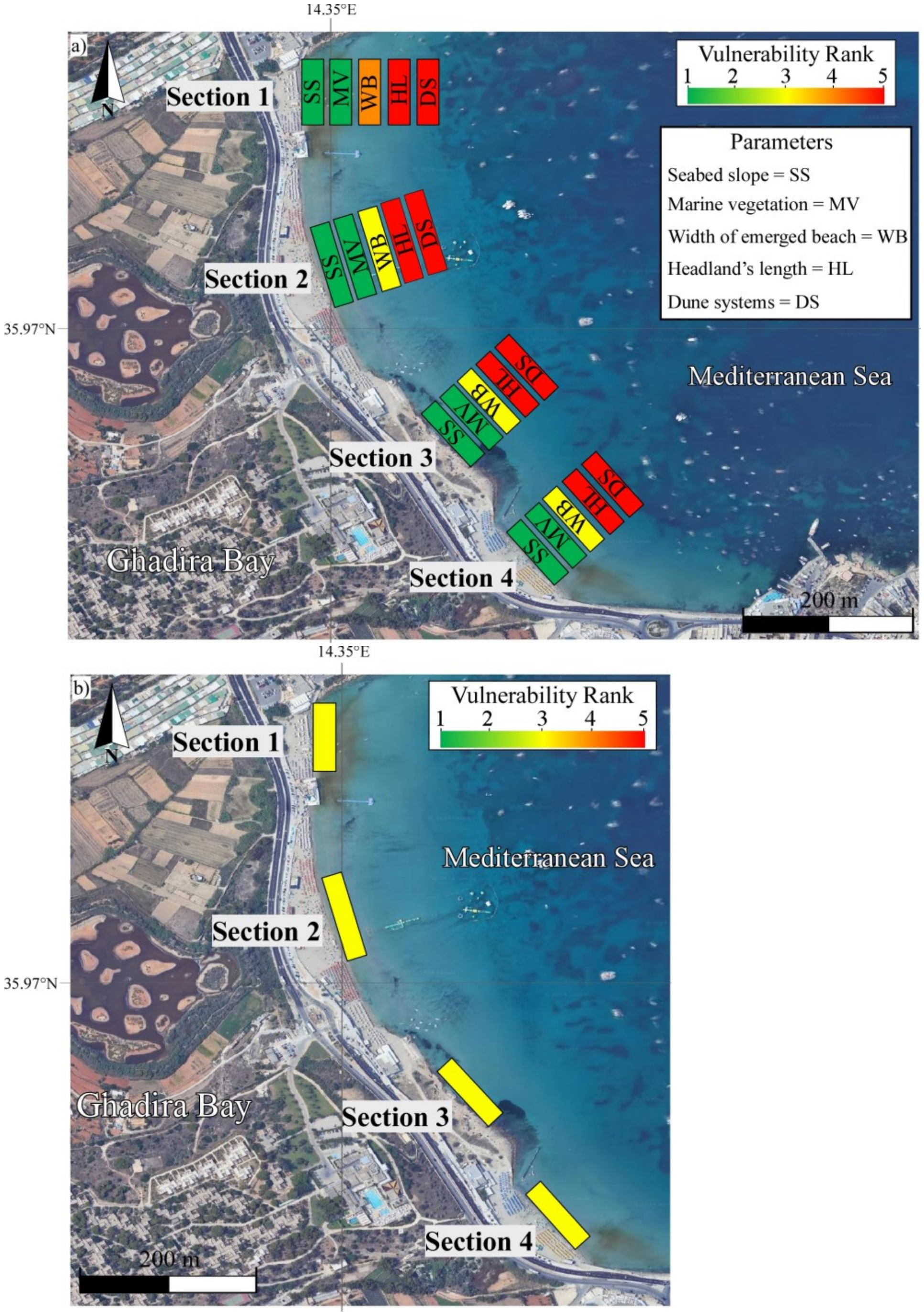
14.35°E
a)
N
Section 1
SS
MV
WB
HL
DS
Vulnerability Rank
1 2 3 4 5
Parameters
Seabed slope = SS
Marine vegetation = MV
Width of emerged beach = WB
Headland's length = HL
Dune systems = DS
Section 2
35.97°N
Mediterranean Sea
Section 3
Ghadira Bay
Section 4
200 m
14.35°E
b)
Section 1
Section 2
Section 3
Section 4
Ghadira Bay
Mediterranean Sea
35.97°N
200 m

Figure 5.

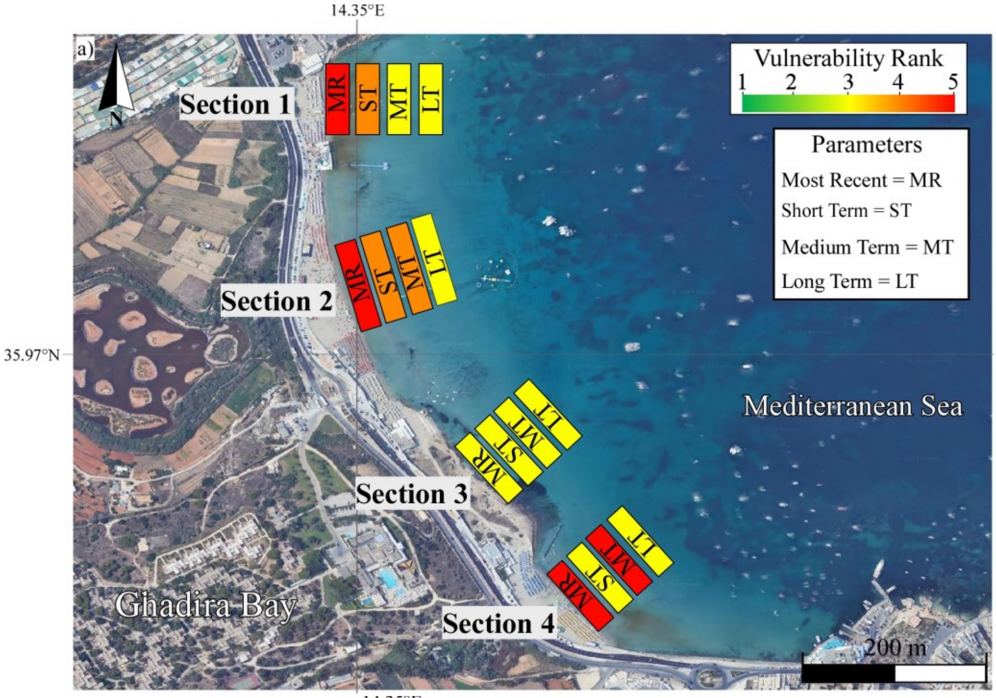
14.35°E
a)
Vulnerability Rank
1 2 3 4 5
Section 1
MR
ST
MT
LT
Parameters
Most Recent = MR
Short Term = ST
Medium Term = MT
Long Term = LT
Section 2
35.97°N
Mediterranean Sea
Section 3
Ghadira Bay
Section 4
200 m
N

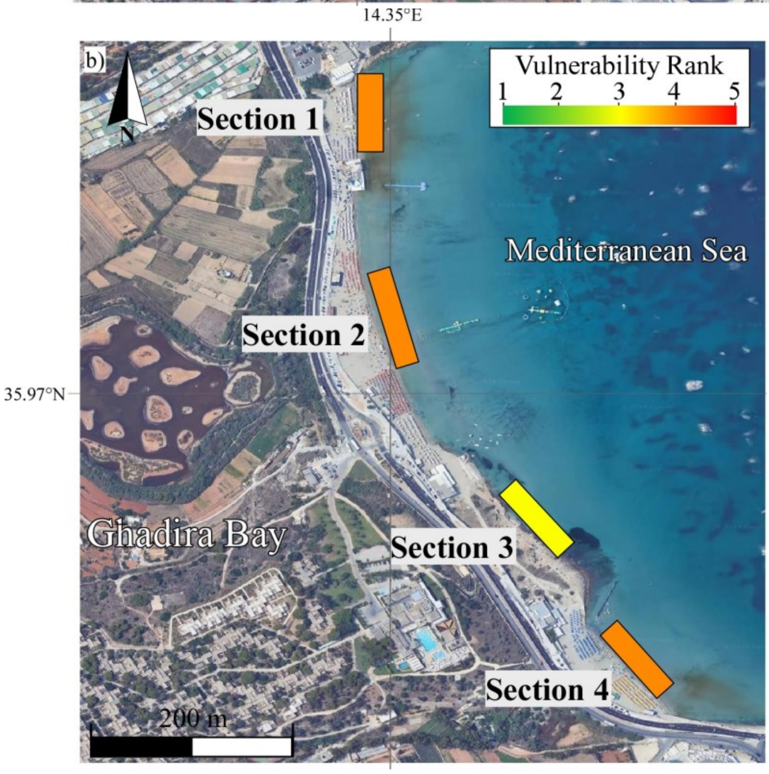
14.35°E
b)
Vulnerability Rank
1 2 3 4 5
Section 1
Mediterranean Sea
Section 2
35.97°N
Ghadira Bay
Section 3
Section 4
200 m
N

Figure 6.

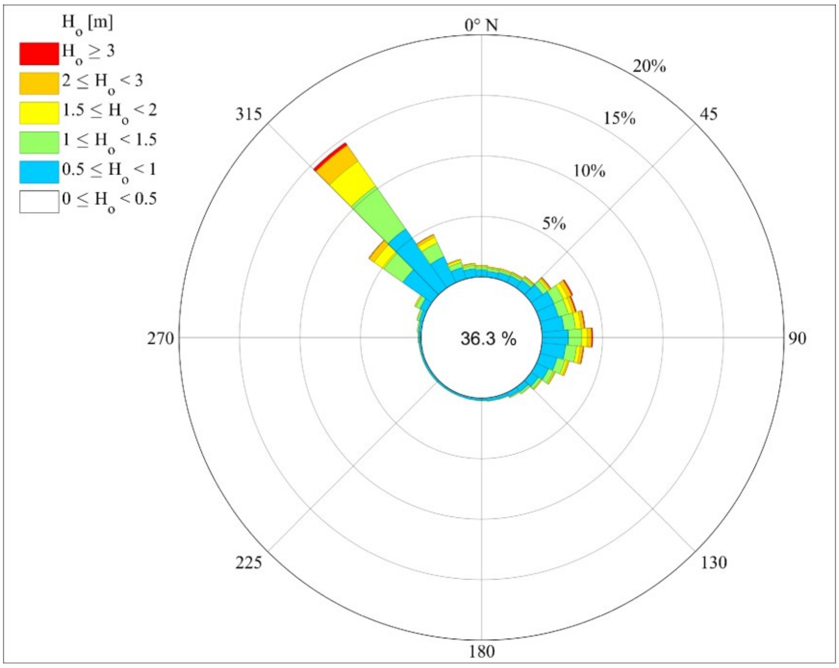

H_o [m]
$H_o \geq 3$
$2 \leq H_o < 3$
$1.5 \leq H_o < 2$
$1 \leq H_o < 1.5$
$0.5 \leq H_o < 1$
$0 \leq H_o < 0.5$
0° N
20%
15%
10%
5%
45
315
270
90
36.3 %
225
130
180

Figure 7.

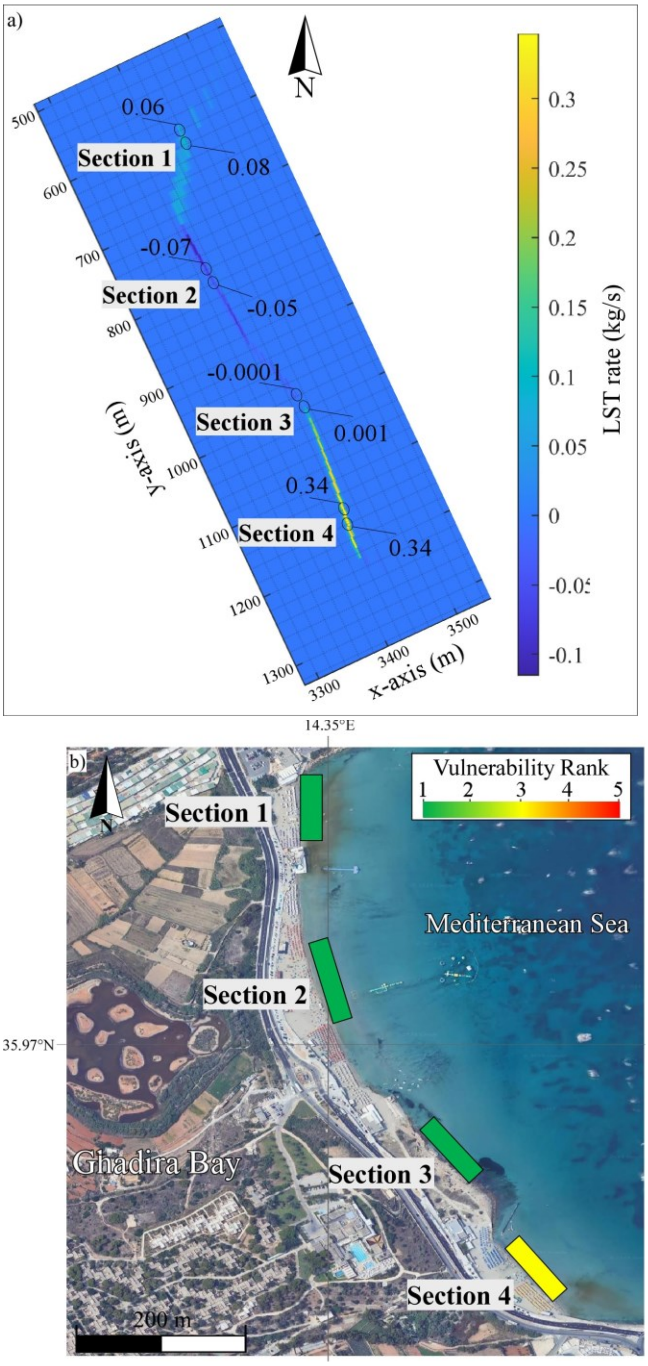

a)
N
0.06
0.08
Section 1
-0.07
-0.05
Section 2
-0.0001
0.001
Section 3
0.34
0.34
Section 4
y-axis (m)
x-axis (m)
LST rate (kg/s)
b)
14.35°E
35.97°N
Vulnerability Rank
1 2 3 4 5
Section 1
Section 2
Section 3
Section 4
Mediterranean Sea
Ghadira Bay
200 m

Figure 8.

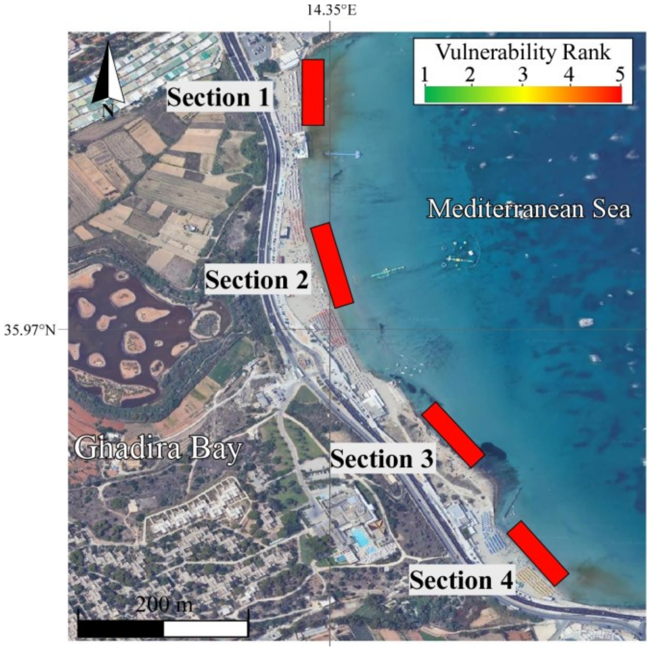
14.35°E
35.97°N
Vulnerability Rank
1 2 3 4 5
Section 1
Section 2
Section 3
Section 4
Mediterranean Sea
Ghadira Bay
N
200 m

Figure 9.

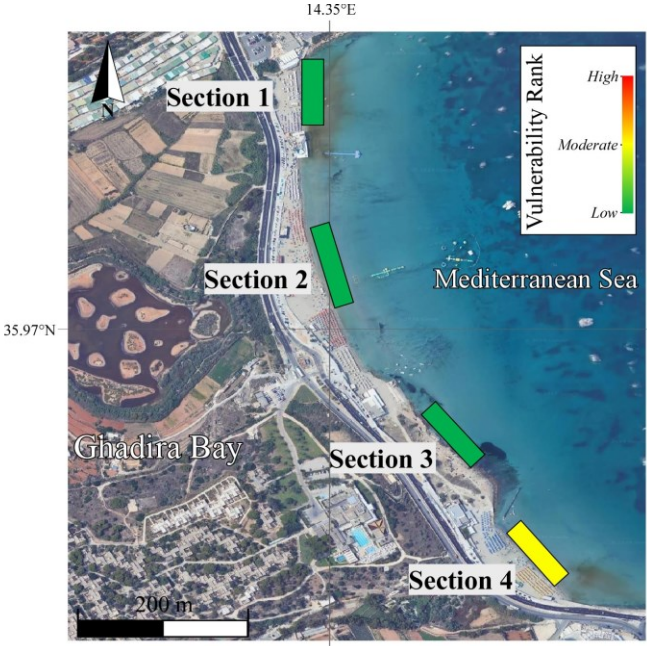
14.35°E
35.97°N
Section 1
Section 2
Section 3
Section 4
Vulnerability Rank
High
Moderate
Low
Mediterranean Sea
Ghadira Bay
200 m
N

Conclusions

This thesis provided a Coastal Vulnerability Index (CVI) designed to assess the vulnerability of coastal areas to erosion at the beach scale. The proposed CVI integrates four key sub-indexes (Morphological Characteristics, Shoreline Displacement, Longshore Sediment Transport and Wave Height) that control coastal erosion. The sub-indexes were analysed through a comprehensive dataset, including aerial surveys, digital elevation models, and wave climate data, supported by numerical modelling through the XBeach 2DH model.

The research project consists of two studies. The first one evaluated the predictive capacity of three widely used bulk formulas (CERC, 1984; Kamphuis, 1991; Van Rijn, 2014) and the XBeach 2DH model to estimate the LST rate across three coastal areas: Għadira Bay (Malta), Cefalù, and Campofelice di Roccella (Sicily). Findings indicated that the XBeach 2DH model achieved greater accuracy due to its ability to account for site-specific factors. Although commonly used, the bulk formulas overestimated LST rates with significant error factors compared to field data, whereas the XBeach model provided notably more accurate predictions, closely corresponding with field measurements.

The second study tested the CVI to assess erosion vulnerability of the Għadira Bay. The methodology revealed that most sections of the bay exhibit low vulnerability, with one section showing moderate vulnerability due to elevated LST rates. This approach overcomes the limitations of previous studies by incorporating factors such as headland length and marine vegetation presence, which are critical elements for sediment balance. Moreover, this study highlighted the necessity of using an accurate method for calculating the LST, following the method proposed in the first study, as the LST represents the most influential factor in assessing the vulnerability to erosion.

In conclusion, the CVI developed in this project provides a tool for assessing the coastal vulnerability to erosion. Integrating sedimentary and morphological data using the numerical model and calculating indexes related to coastal erosion provided a comprehensive and reliable representation of beach erosion vulnerability. Research findings enhance the importance of accurate and practical estimations to support coastal management decision-making in mitigating risks associated with coastal erosion.